AGU PUBLICATIONS

Tectonics

RESEARCH ARTICLE
10.1002/2015TC003937

Key Points:
- Kinematic and thermochronological study of interacting neighboring orogens
- Two stages of extensional exhumation influenced the Alpine-Dinaridic junction
- Structures of the Alps extend far into the Dinarides

Correspondence to:
I. E. van Gelder,
i.e.vangelder@uu.nl

Citation:
van Gelder, I. E., L. Matenco, E. Willingshofer, B. Tomljenović, P. A. M. Andriessen, M. N. Ducea, A. Beniest, and A. Gruić (2015), The tectonic evolution of a critical segment of the Dinarides-Alps connection: Kinematic and geochronological inferences from the Medvednica Mountains, NE Croatia, *Tectonics*, *34*, 1952–1978, doi:10.1002/2015TC003937.

Received 5 JUN 2015
Accepted 21 AUG 2015
Accepted article online 26 AUG 2015
Published online 28 SEP 2015

The tectonic evolution of a critical segment of the Dinarides-Alps connection: Kinematic and geochronological inferences from the Medvednica Mountains, NE Croatia

I. E. van Gelder[1,2], L. Matenco[1], E. Willingshofer[1], B. Tomljenović[3], P. A. M. Andriessen[2], M. N. Ducea[4,5], A. Beniest[1], and A. Gruić[3]

[1]Faculty of Geosciences, Utrecht University, Utrecht, Netherlands, [2]Faculty of Earth and Life Sciences, VU University Amsterdam, Amsterdam, Netherlands, [3]Faculty of Mining, Geology & Petroleum Engineering, University of Zagreb, Zagreb, Croatia, [4]Department of Geosciences, University of Arizona, Tucson, Arizona, USA, [5]Faculty of Geology and Geophysics, University of Bucharest, Bucharest, Romania

Abstract The transition zone between the Alps and Dinarides is a key area to investigate kinematic interactions of neighboring orogens with different subduction polarities. A study combining field kinematic and sedimentary data, microstructural observations, thermochronological data (Rb-Sr and fission track), and regional structures in the area of Medvednica Mountains has revealed a complex polyphase tectonic evolution. We document two novel stages of extensional exhumation. The first stage of extension took place along a Late Cretaceous detachment following the late Early Cretaceous nappe stacking, burial, and greenschist facies metamorphism. Two other shortening events that occurred during the latest Cretaceous-Oligocene were followed by a second event of extensional exhumation, characterized by asymmetric top-NE extension during the Miocene. Top-NW thrusting took place subsequently during the Pliocene inversion of the Pannonian Basin. The Cretaceous nappe burial, Late Cretaceous extension, and the Oligocene(-Earliest Miocene) contraction are events driven by the Alps evolution. In contrast, the latest Cretaceous-Eocene deformation reflects phases of Dinaridic contraction. Furthermore, the Miocene extension and subsequent inversion display kinematics similar with observations elsewhere in the Dinarides and Eastern Alps. All these processes demonstrate that the Medvednica Mountains were affected by Alpine phases of deformations to a much higher degree than previously thought. Similarly with what has been observed in other areas of contractional polarity changes, such as the Mediterranean, Black Sea, or New Guinea systems, the respective tectonic events are triggered by rheological weak zones which are critical for localizing the deformation created by both orogens.

1. Introduction

The interaction between neighboring orogens with different subduction polarities is often related to geodynamic settings of retreating subducted slabs and associated extensional back-arc basins [*Doglioni et al.*, 1999; *Faccenna et al.*, 2013; *Jolivet and Faccenna*, 2000]. Such interactions are commonly described in studies of Mediterranean orogens [e.g., *Faccenna et al.*, 2004; *Kissling et al.*, 2006]. Rollback subduction associated with back-arc extension affected transitional areas between the Alps and Apennines, the Alps and Dinarides, the Dinarides and Carpatho-Balkanides, the Hellenides-Aegean, Black Sea and Anatolian tectonics. In all these situations, the back-arc extension postdated an inherited subduction and/or collisional nappe stack and was accompanied by large-scale rotations, displacements along the orogenic strike, and formation of highly arcuate mountain chains [e.g., *Faccenna et al.*, 2004, 2005; *Luth et al.*, 2013; *Matenco et al.*, 2010; *Munteanu et al.*, 2014; *Schmid and Kissling*, 2000].

We investigate one interesting area where such kinematic interactions of neighboring orogens were observed, namely the transition zone between the Alps and Dinarides (Figure 1a), which are orogens with different subduction polarities (Adria the upper plate in the Alps versus Adria the lower plate in the Dinarides) [e.g., *Schmid et al.*, 2008]. A Cretaceous-Paleogene phase of orogenic buildup took place in both mountain belts and was followed by a Miocene period of extension associated with the formation of the Pannonian back-arc basin, driven by the rapid Miocene subduction rollback of the Carpathian slab [e.g., *Horváth et al.*, 2006].

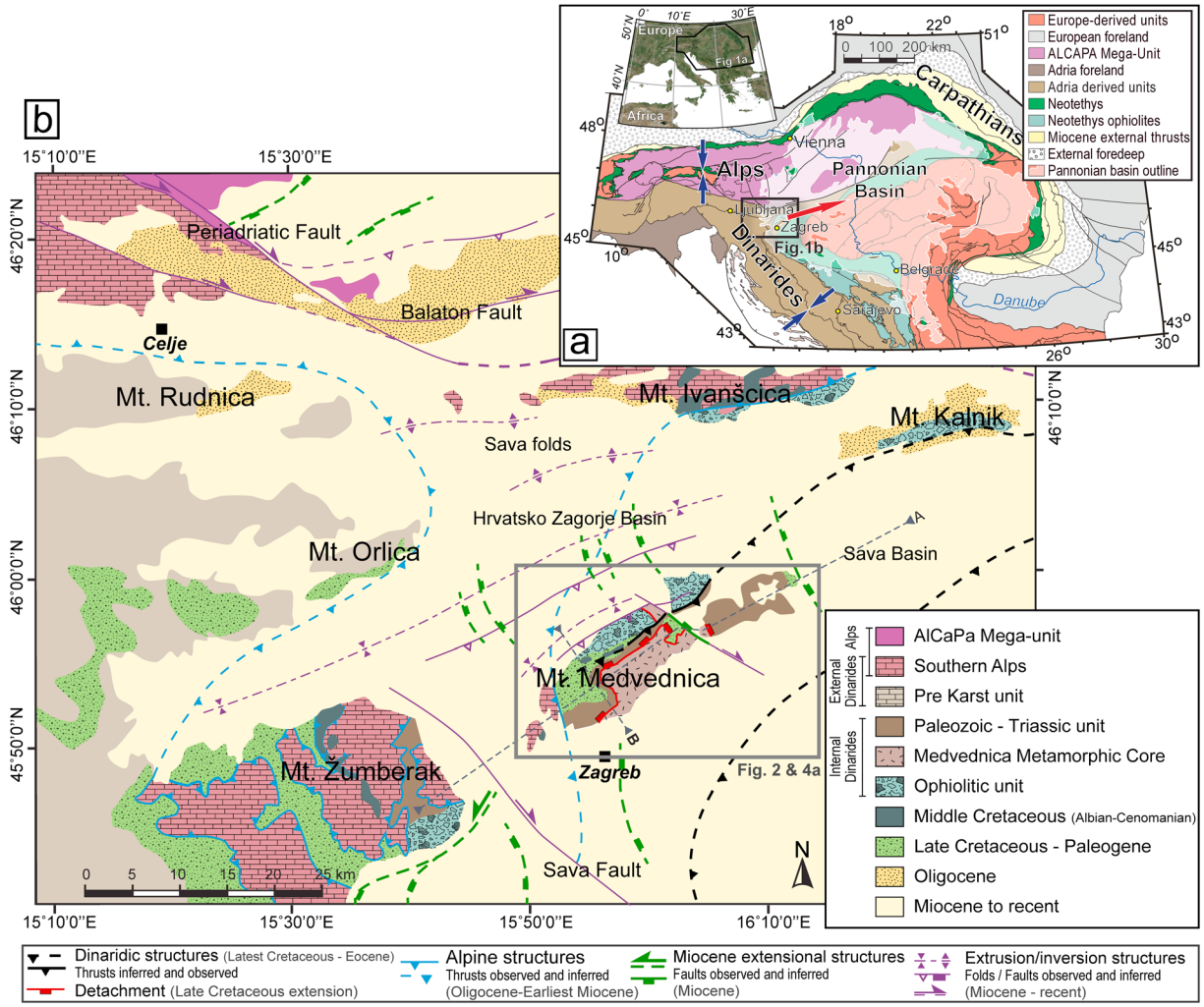

Figure 1. (a) Simplified tectonic map of the Alpine-Carpathian-Dinaric (AlCaDi) system [modified after *Schmid et al.*, 2008]. The red arrow indicates the main direction of extension in the Pannonian basin; the blue arrows indicate the main direction of contraction for the Alps and the Dinarides. The geographical location of the AlCaDi system is shown in the inset figure. (b) Tectonostratigraphic map of the Medvednica Mountains and surrounding areas near the Alpine-Dinaridic junction [simplified and modified from *Haas et al.*, 2000; *Lužar-Oberiter et al.*, 2012; *Matoš et al.*, 2014; *Tomljenović and Csontos*, 2001, with the results of this study]. Location of figure is displayed in Figure 1a.

In the Pannonian Basin, a number of "inselbergs" expose Paleozoic-Mesozoic sediments deformed during Cretaceous-Paleogene times and are surrounded by Miocene sediments [e.g., *Csontos and Vörös*, 2004; *Tomljenović et al.*, 2008; *Ustaszewski et al.*, 2008]. One such inselberg is the Medvednica Mountains of northern Croatia that is located in the transitional area between the Alps and Dinarides (Figures 1b and 2). This inselberg exposes a Cretaceous-Paleogene nappe stack composed of metamorphosed and nonmetamorphosed Paleozoic-Mesozoic sediments [e.g., *Pamić*, 2002; *Pamić and Tomljenović*, 1998; *Tomljenović et al.*, 2008]. Particularly interesting is the observation that Upper Cretaceous sediments of unclear genesis show strikingly similar stratigraphic and facies characteristics when compared with the coeval synorogenic deposits of the Eastern Alps (i.e., the Gosau sediments) [e.g., *Wagreich and Faupl*, 1994; *Judik et al.*, 2008; *Willingshofer et al.*, 1999a].

Previous kinematic studies of the Medvednica Mountains have inferred a Cretaceous-Paleogene period of Dinaridic nappe stacking that was followed by Miocene extension, accompanied by transcurrent deformation and by an inversion starting during Pliocene times [e.g., *Tomljenović et al.*, 2008; *Vrabec and Fodor*, 2005].

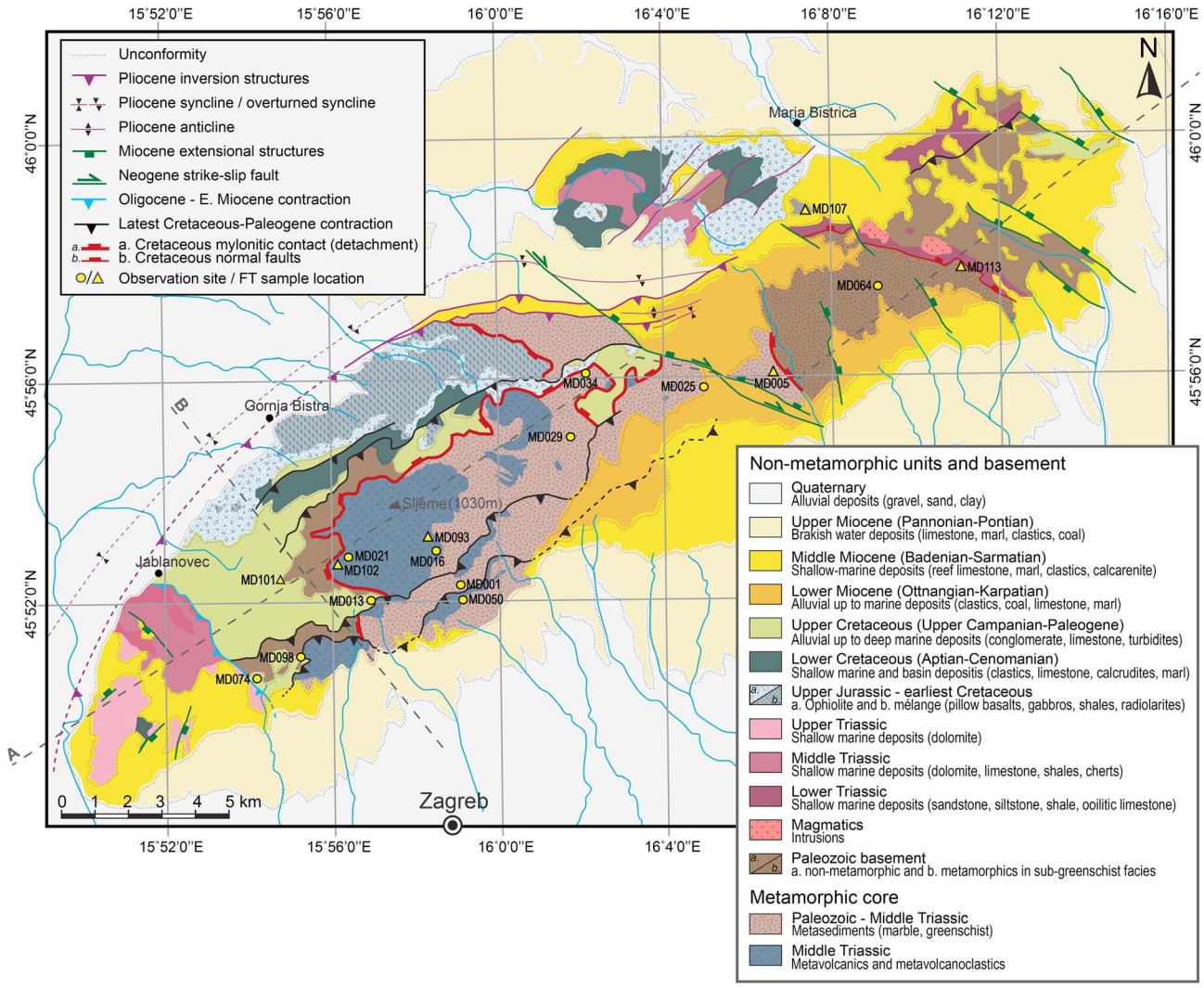

Figure 2. Geological map of the Medvednica Mountains [compiled from *Basch*, 1995; *Matoš et al.*, 2014; *Tomljenović et al.*, 2008, and the results of the present study]. The map shows sample locations used for Rb-Sr and apatite/zircon fission track dating, as well as the location of the cross sections A and B (see Figure 9). The location of the figure is displayed in Figure 1b.

Other inselbergs located more to the east along the strike of the Dinarides display Miocene extensional detachments. These detachments have exhumed previously stacked and metamorphosed Adriatic units in their footwalls [e.g., *Matenco and Radivojević*, 2012; *Stojadinović et al.*, 2013; *Toljić et al.*, 2013; *Ustaszewski et al.*, 2010]. The Miocene extension observed in the Eastern Alps near their transition to the Pannonian Basin is also associated with detachments exhuming previously metamorphosed units, such as the Rechnitz window [e.g., *Cao et al.*, 2013; *Tari et al.*, 1992, 1999; *Ratschbacher et al.*, 1991]. The kinematics of such Miocene exhumation in the Medvednica Mountains and in the larger transitional area between the Alps and Dinarides is still unclear.

We aim to discriminate the effects of the Alpine and Dinaridic tectonic evolution in the buildup of the Medvednica Mountains by constraining their kinematic, metamorphic, and depositional history. To this aim, we have analyzed the structural, sedimentological, and exhumation characteristics of the Late Cretaceous deposition, Cretaceous-Paleogene nappe stacking, and the Miocene extension followed by the subsequent inversion. The methodology employed combines field kinematics, studying depositional characteristics, microstructural observations, thermochronological data (Rb-Sr and apatite and zircon fission track), and integration with previously observed regional to microscale structures.

2. The Tectonic Evolution of Dinaridic-Alpine Transitional Area

The Dinarides formed in response to the Jurassic-Cretaceous subduction and closure of the Neotethys Ocean during Adria-Europe convergence [*Pamić*, 2002; *Schmid et al.*, 2008; *Ustaszewski et al.*, 2010]. The Middle Triassic onset of Neotethys opening was associated with intermediate and basic volcanism and the formation of the Adriatic passive continental margin [*Pamić*, 1984; *Schmid et al.*, 2008]. Transition from dominantly carbonatic Upper Triassic facies into more pelagic Middle Jurassic facies indicates a gradual deepening of the former Adriatic passive margin from the SW to NE in the present-day geometry [e.g., *Dimitrijević*, 1997; *Schefer et al.*, 2011; *Toljić et al.*, 2013]. The subsequent early Middle Jurassic intraoceanic subduction [*Schmid et al.*, 2008] was followed by the Late Jurassic-Earliest Cretaceous emplacement of ophiolites and associated Jurassic ophiolitic mélange during their obduction over the eastern Adriatic passive margin (i.e., the Western Vardar ophiolites) [*Dimitrijević*, 1997; *Karamata*, 2006; *Pamić*, 2002; *Babić et al.*, 2002; *Schmid et al.*, 2008]. The subduction of the Adriatic plate and the continental collision with the overriding Europe-derived Tisza-Dacia megaunit are recorded by successive Cretaceous-Paleogene phases of shortening. Following an earlier late Early Cretaceous onset of contraction, the latest Cretaceous-Eocene shortening and collision is associated with the formation of the Sava suture zone between European- and Adriatic-derived units, widespread magmatism, and nappe stacking in the former Adriatic passive continental margin. The deformation continued by a gradual migration of shortening toward the foreland, where the main Eocene Dinaric event is well documented in numerous studies [*Dimitrijević*, 1997; *Pamić*, 1993, 2002; *Pamić and Balen*, 2001; *Schmid et al.*, 2008; *Ustaszewski et al.*, 2010]. The Dinaridic nappe stack contains a number of thin- and thick-skinned thrust sheets that are generically grouped into the External Dinarides and Internal Dinarides. In the latter, the three most internal units carry in a structurally higher position the earlier obducted ophiolites and ophiolitic mélanges (Figure 1). The nappe contacts are often marked by the deposition of syncontractional turbidites (i.e., flysch deposits) [e.g., *Dimitrijevic and Dimitrijevic*, 1987], which become progressively younger in the SW direction [e.g., *Tari*, 2002]. Along the strike of the orogen, most of the Internal Dinaridic units wedge out laterally toward the NW (Figure 1a), i.e., toward the area of the Medvednica Mountains.

North of the Dinarides, the Tisza unit separated from Europe during Middle Jurassic times and drifted southward to a position close to the Adriatic units, as inferred by faunal assemblages with Mediterranean affinity [*Haas and Péró*, 2004]. Tisza was subsequently realigned with another European-derived unit (i.e., Dacia) during the late Early Cretaceous closure affecting the NE part of the Neotethys Ocean (Figure 1a) [*Csontos and Vörös*, 2004; *Schmid et al.*, 2008]. The Tisza-Dacia megaunit formed the upper plate of the Late Cretaceous-Eocene subduction and collision recorded by the Dinarides. West of Tisza, the Alps formed in response to the Cretaceous-Paleogene southward subduction and collision of the Alpine Tethys and its European continental margin [e.g., *Neubauer et al.*, 1999; *Schmid et al.*, 2008]. In the areas WNW of the Medvednica Mountains (Figure 1), the Southern and Julian Alps recorded Eocene NE-SW shortening (the Dinaric phase of deformation) that was subsequently followed by Oligocene-Miocene southward thrusting (Alpine phase of deformation) [e.g., *Castellarin et al.*, 1992; *Doglioni and Bosellini*, 1987; *Placer*, 1999]. The Miocene shortening was coeval with large-scale dextral displacements along the peri-Adriatic lineament separating the Eastern and Southern Alps (such as the Balaton line, Sava and Drava faults in the vicinity of the Medvednica Mountains, Figure 1b) [*Fodor et al.*, 2005; *Placer*, 1999; *Tomljenović and Csontos*, 2001].

The dextral displacements in the Dinaridic-Alpine transition zone and associated lateral extrusion of the Eastern Alps were partly coeval with the back-arc extension of the Pannonian Basin starting at around 20 Ma [e.g., *Horváth et al.*, 2015; *Tari and Pamić*, 1998] that created a number of deep half-grabens along the SW margin of the Pannonian Basin, among which the largest ones are the Hrvatsko Zagorje, Sava, and Drava basins (Figure 1b) [*Pavelić*, 2001; *Saftić et al.*, 2003]. These extensional features were subsequently affected by contraction during the Pliocene-Quaternary inversion of the Pannonian Basin [e.g., *Tomljenović and Csontos*, 2001; *Bada et al.*, 2007; *Ustaszewski et al.*, 2014].

2.1. The Architecture of the Medvednica Mountains

The Medvednica Mountains are composed of a metamorphic core overlain by nonmetamorphic Mesozoic and Cenozoic deposits (Figure 2). The center of the metamorphic core is metamorphosed in greenschist facies, while toward its margins, it comprises Paleozoic sediments that are affected by a very low degree of

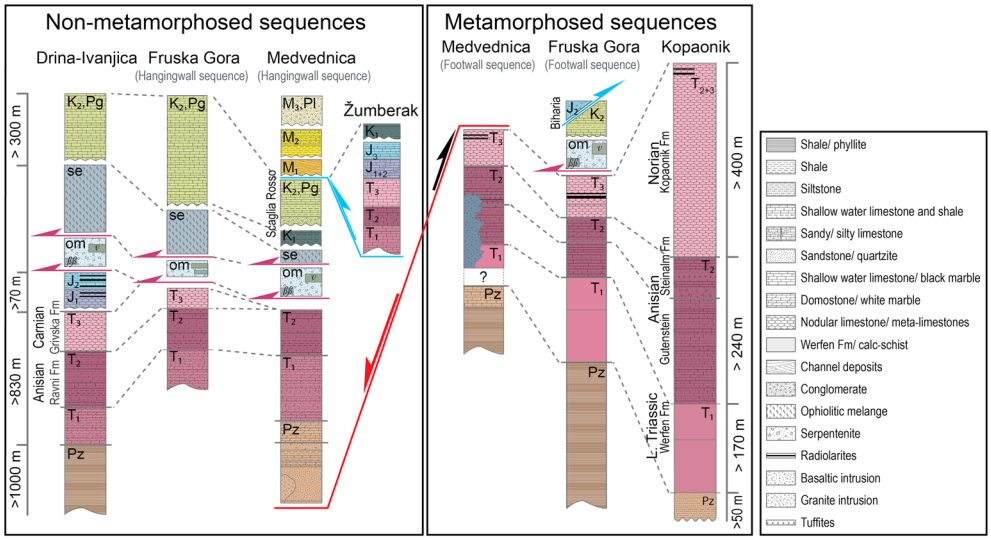

Figure 3. Tectonostratigraphic columns with a correlation between the metamorphic footwall units and the subgreenschist facies to nonmetamorphosed hanging-wall units of the Medvednica Mountains [compiled from *Halamić and Goričan*, 1995; *Halamić et al.*, 2001; *Tomljenović et al.*, 2008] with the similar sequences in the Fruška Gora [modified after *Toljić et al.*, 2013] and with synthetic tectonosedimentary columns of Drina Ivanjica and Kopaonik of Serbia [modified after *Dimitrijević*, 1997] [simplified after *Schefer et al.*, 2011]. For the colour coding of the tectonic features, please refer to Figure 10. Abbreviations: Upper Paleozoic (Pz), Lower Triassic (T_1), Middle Triassic (T_2), Upper Triassic (T_3), Lower Jurassic (J_1), Middle Jurassic (J_2), ophiolitic mélange (om), serpentinite (se), Lower Cretaceous (K_1), Upper Cretaceous (K_2), Paleogene (Pg), Middle Miocene (M_2), Upper Miocene (M_3), Pliocene (Pl).

metamorphism, mostly subgreenschist facies. All units are truncated by normal and reverse faults and are surrounded by the Miocene-Quaternary sediments of the Pannonian Basin (Figure 2).

The greenschist facies metamorphic core is composed of two distinct lithologies, a metavolcanic series and a metasedimentary series [*Lugović et al.*, 2006; *Tomljenović et al.*, 2008, and references therein]. The metavolcanic series is dominantly made up of chloritic schists that have still preserved in few places their original basaltic or intermediate volcanic protolith. The metasedimentary series contains in its lower part dark phyllites with rare intercalations of quartzites, overlain by massive marbles, carbonatic schists, metagreywackes, metaconglomerates, and fine-grained quartzites derived from the metamorphism of radiolarites [*Basch*, 1995; *Tomljenović*, 2002]. Locally, the metavolcanics are interlayered with marbles, which is an effect of isoclinal folding combined with an original multilayered stratigraphy. Biostratigraphic and radiometric dating of the metamorphic core indicate that the metavolcanics have a protolith age of Middle to Upper Triassic [*Belak et al.*, 1995] and the metasediments have an age range from Devonian up to Upper Triassic [*Đurđanović*, 1973; *Šikić et al.*, 1977].

Near the margins of the metamorphic core, subgreenschist facies Paleozoic metasediments are mostly pelagic shales, turbidites, and carbonates. Other biostratigraphic dating analyzing both the protolith of the greenschist facies metamorphic core and the flanking Paleozoic metasediments indicate Silurian to Late Triassic ages [*Đurđanović*, 1973; *Sremac and Mihajlović-Pavlović*, 1983]. In the NE corner of the Medvednica Mountains, clastic-carbonatic sediments metamorphosed in greenschist facies are reported as Permian in age (Figure 2) [*Basch*, 1995]. The Paleozoic metasediments are unconformably covered by a nonmetamorphosed Upper Permian-Triassic dominantly carbonatic sequence (Figures 2 and 3). A thick Triassic succession of shallow-marine clastics and carbonates is thrusted over the Paleozoic and Cretaceous sediments in the SW part of the mountains, forming the highest pre-Neogene tectonic unit (i.e., the Žumberak nappe of *Tomljenović et al.* [2008]). In the NW part of the mountain, a chaotic assemblage of blocks of metamagmatic, greywackes, radiolarites, limestones, sandstones, and turbidites are embedded together with blocks of ophiolites in a shaly silt matrix (Figure 2) [*Pamić and Tomljenović*, 1998]. Biostratigraphic dating of blocks of radiolarites has yielded Upper Ladinian-Carnian and Upper Bajocian-Lower Callovian ages [*Halamić and Goričan*, 1995; *Halamić et al.*, 1999], while scarce fauna in the matrix has been dated as Lower Jurassic to Bajocian [*Babić et al.*, 2002]. This assemblage has been interpreted as an ophiolitic melange, part of the

Western Vardar Ophiolites obducted during Late Jurassic-Earliest Cretaceous times [*Schmid et al.*, 2008, and references therein].

The metamorphosed Paleozoic-Triassic sequence and the ophiolitic mélange are unconformably covered by Upper Cretaceous-Paleocene sediments (Figure 3). These show a gradual transgressive pattern from massive conglomerates and alluvial fan deposits at the base to sandstones and Scaglia Rossa hemipelagic carbonates higher up in the sequence [*Babić et al.*, 1976; *Crnjaković*, 1980; *Lužar-Oberiter et al.*, 2012]. These deposits are stratigraphically continuous with the uppermost Cretaceous turbidites (carbonatic and clastic) that are commonly observed elsewhere along the Sava suture zone [e.g., *Ustaszewski et al.*, 2010]. Based on similar biostratigraphic ages and lithofacies characteristics, these Upper Cretaceous sediments are often referred to as Gosau deposits [*Borojević Šostarić et al.*, 2012; *Judik et al.*, 2006; *Tomljenović et al.*, 2008] analogous to coeval and similar deposits widely observed in the Eastern Alps. There, the deposition of Gosau sediments is driven either by synorogenic normal faulting or by the evolution of thrust sheet top basins [*Krohe*, 1987; *Neubauer et al.*, 1995; *Ortner*, 2001; *Wagreich and Decker*, 2001]. In contrast, some of the deposits attributed to the Gosau formation in the Dinarides were deposited in the footwall of the main thrusts and are overlain by deep-water syncontractional turbidites [*Dimitrijević*, 1997; *Matenco and Radivojević*, 2012]. These deposits have been related to subsidence postdating the late Early Cretaceous contraction.

The pre-Neogene units of the Medvednica Mountains are unconformably overlain by the Miocene sediments of the Pannonian Basin (Figure 2). Their biostratigraphy is described by using the regional timescale of the endemic Paratethys [e.g., *Magyar et al.*, 1999; *Rögl*, 1999; *Steininger and Wessely*, 1999; *Steininger et al.*, 1988]. These Miocene-Lower Pliocene sediments are truncated by normal faults, postdate some thrust faults while being truncated by others, and dip away at low angles from the mountains along the SE, NE, and SW flanks (Figure 2) [*Basch*, 1995; *Šikić et al.*, 1977]. Along the NW flank of Medvednica Mountains, these strata are locally brought to a (sub)vertical position, which is the result of the thrusting starting with Pliocene times (Figure 2) [*Tomljenović et al.*, 2008]. This event is observed by NE-SW oriented thrusts and kilometer-scale folds and documented by seismic interpretation studies combined with surface observations [e.g., *Tomljenović and Csontos*, 2001; *Tomljenović*, 2002].

2.2. Tectonic Evolution of the Medvednica Mountains

The kinematic evolution of the Medvednica Mountains has been generally described in terms of either three deformational events [*Jamičić*, 2000] or five such events postdating the Late Jurassic-earliest Cretaceous obduction [*Tomljenović et al.*, 2008]. In the latter interpretation, an initial late Early Cretaceous nappe stacking and burial event occurred oblique to the former Adriatic passive continental margin and was followed by Early Albian thrusting. The Middle Eocene-Oligocene deformation continued as a result of the collision and thrusting of Tisza over the turbidites of the Sava zone and was accompanied or followed by right-lateral shearing of the Sava zone during the Eocene-Oligocene [*Tomljenović et al.*, 2008]. These latter deformations were associated with up to 130° clockwise rotations that peaked in Oligocene-Early Miocene times. This overall complex history was followed by widespread Miocene normal faulting crosscutting all earlier structures (Figure 2), while the thrusting starting with Pliocene times uplifted the mountains to their present elevations. The latter was accompanied by up to 30° counterclockwise rotations that started probably in the late Early Miocene and continued in post-Miocene times controlled by indentation and counterclockwise rotation of the Adriatic plate [e.g., *Márton et al.*, 2002; *Tomljenović and Csontos*, 2001; *Tomljenović et al.*, 2008].

The initial nappe stacking during the late Early Cretaceous is associated with peak metamorphic conditions. The metavolcanics from the greenschist facies metamorphic core indicate peak metamorphism between 135 and 122 Ma based on Ar/Ar dating of white micas [*Borojević Šostarić et al.*, 2012]. The associated PT conditions were in the order of 350–410°C and 3–4 kbar [*Judik et al.*, 2006, 2008; *Lugović et al.*, 2006]. K-Ar dating of muscovite from metasediments in the metamorphic core suggested that the period of peak metamorphism took place until 110 Ma [*Belak et al.*, 1995; *Judik et al.*, 2006, 2008]. Furthermore, Ar/Ar dating of the metavolcanics inferred a younger age of 80 Ma that overprinted the peak metamorphism. This younger age was interpreted to be related to the period of Late Cretaceous contraction associated with subsidence in the Gosau-type basins [*Borojević Šostarić et al.*, 2012]. K-Ar illite dating in the subgreenschist facies metamorphosed sequence yielded ages between 124 and 95 Ma [*Belak et al.*, 1995; *Judik et al.*, 2006]. In these latter rocks, peak temperatures are in the range of 100–240°C based on organic thermometers sampled in the ophiolitic mélange and the Cretaceous-Paleocene deposits [*Judik et al.*, 2008].

3. Kinematic Analysis

We have focused the kinematic analysis on major structures, such as nappe contacts or detachments, which are essential for understanding the contractional, burial, and subsequent exhumation of the Medvednica metamorphic core. We particularly investigated the contact zone between the greenschist facies metamorphic core and the surrounding subgreenschist facies to nonmetamorphic Paleozoic-Triassic sediments. The field data include measurements of foliations, stretching lineations, and associated kinematic indicators and the analysis of folding geometries. Furthermore, brittle structures were measured together with kinematic indicators, such as slickensides, Riedel shears, or drag folds. The chronology of deformation was derived in a first stage from superposition criteria such as crosscutting relations of foliations, or superposition of folding. Further timing constraints were subsequently derived from thermochronology and available biostratigraphic data. Field observations were supplemented by microstructural analysis and petrological observations in order to correlate deformation events and to infer pressure-temperature conditions.

The oldest deformational structures recorded in the Medvednica Mountains are observed in the very low, subgreenschist metamorphic facies to almost nonmetamorphosed Paleozoic sediments surrounding the greenschist facies metamorphosed core. These structures, which are characterized by isoclinal folding and a pervasive axial plane cleavage, were in particular well observed in Paleozoic dark shales and distal turbidites. Such structures were not observed in the unconformably overlying metamorphosed Paleozoic-Triassic sediments. Similar structures were commonly observed in the low to very low degree Paleozoic metamorphic basement elsewhere in the Dinarides, formed in response to (late) Variscan deformation [e.g., *Filipović et al.*, 2003]. This deformation event is outside the scope of our study and will not be discussed further.

3.1. D1: Burial and Peak Metamorphism

In the greenschist facies part of the metamorphic core, the oldest phase of deformation (D1) is characterized by a pervasive foliation (S1) (Figure 5a) that is (sub)parallel to the bedding planes and to the axial planes of a first stage of isoclinal folds (F1). The S1 is mainly observed by small-scale structures (up to decimeters), which is evident in particular by the alternation of metalimestones and volcanics. These were intercalated in the original stratigraphy and were subsequently isoclinally folded (Figure 5a). Coeval NW-SE trending stretching lineations (L1) were deformed subsequently by folding and shearing together with the F1 folds. Shear sense criteria observed in outcrops and thin sections indicate both top-NW and top-SE senses of shear (Figure 4). The D1 lineations, folds, and foliation are all affected by subsequent deformation events.

In thin sections, the S1 foliation (Figure 5b) is pervasive and associated with coaxial flattening in particular in marbles or calc-schists. The coaxial deformation is expressed by elongation of quartz and calcite (aspect ratios of 1:7) with a preferred orientation of the *c* axis. The analysis of thin sections of metavolcanic rocks indicates an original protolith composed of pyroxenes, quartz, plagioclase, biotite, oxides, and olivine, in different percentages. The pyroxenes, olivine, and plagioclase are replaced during metamorphism by epidote and feldspar, indicative for the peak mineralogical assemblage (Figure 5b, sample MD021). The analysis of metasediments in thin sections suggests that the original protolith contained dominantly calcite, feldspar, oxides, plagioclase, quartz, and white micas, in various percentages for different samples analyzed. A constant growth and dynamic recrystallization (e.g., larger growth, bulging, subgrain rotation) of quartz, feldspar, and calcite took place during metamorphism (Figure 5b, sample MD016). The analysis of the peak metamorphic conditions indicate temperatures around 350–400°C representing a greenschist metamorphic facies, which is observed in both the metavolcanics and the metasediments.

3.2. D2: Top-NE Directed Stretching and Retrograde Metamorphism

Our observations demonstrate that a major shear zone separates the greenschist facies part of the metamorphic core from the overlying subgreenschist facies Paleozoic and nonmetamorphosed Mesozoic sediments. The second stage of deformation (D2) is observed in the greenschist facies part of the metamorphic core by pervasive stretching associated with a dominant mylonitic fabric and stretching lineation (L2) (Figure 4a). These stretching lineations are associated with kinematic indicators such as shear bands or sigma clasts indicating a top-NE sense of shear in both outcrops and thin sections (Figures 4b and 5b). In the SW part of the mountains, the senses of shear are roughly top-ENE oriented, while in the NE, they are NNE to NE oriented (Figure 4a). The shearing took place almost parallel with the preexisting foliation affecting

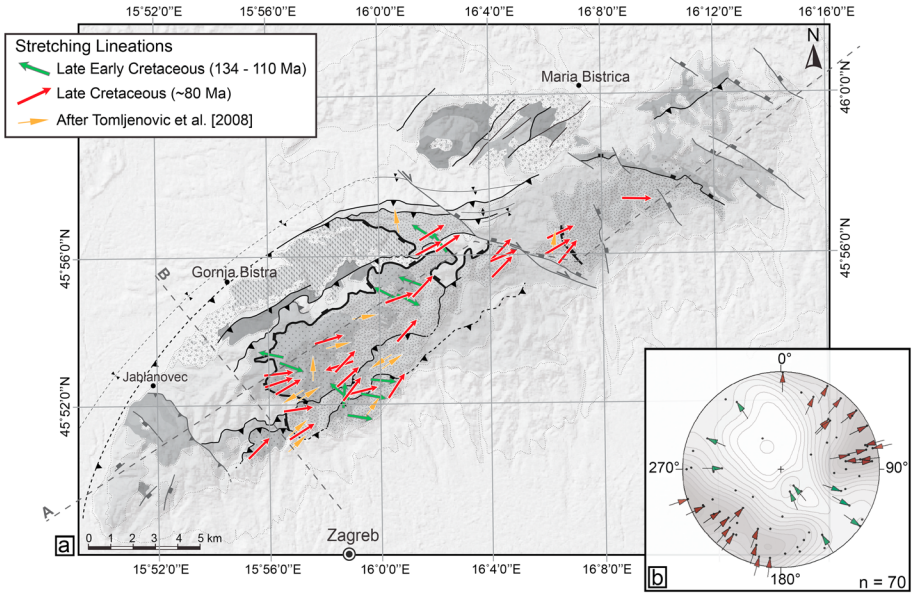

Figure 4. (a) Same geological map as in Figure 2 in grey scale projected over a digital elevation model image of the inselberg, with an overlay of arrows that indicate the observed direction of shearing related to the late Early Cretaceous nappe stacking (green arrows) and Late Cretaceous extensional exhumation (red arrows). Our data on the ductile sense of transport are compared with the previously published ones in *Tomljenović et al.* [2008] (orange arrows). (b) Stereoplot of the main stretching lineations with the tectonic transport of the hanging wall during shearing for D1 (green arrows) and D2 (red arrows) deformations. The total stretching database of ~70 measured D2 stretching lineations is projected as a contour plot that suggests their dominant NE-SW orientation.

pervasively the S1 foliation planes and F1 folds. This is clearly observed in thin sections with renewed growth of chlorite along the S1 planes. Whenever shearing diverges, an S2 foliation plane formed parallel with the L2 stretching lineation. Reactivation of S1 foliation as C-planes to the C-C′ shear bands is often observed to accommodate the top-NE shearing. The mylonites are well developed in particular in the main shear zone at the outer contacts of the greenschist facies part of the metamorphic core (Figure 2). This is obvious in particular when the shearing affected the marbles or calc-schists flanking the metavolcanics that formed often calc-mylonites at the structural contact with the subgreenschist facies Paleozoic metapelites situated in their hanging wall. This contact is furthermore affected by cataclastic shears and tectonic brecciation with similar top-NE kinematics, suggesting shearing during exhumation.

In thin sections, the mylonitic fabric has often a spatial variance in strain accommodation, expressed by alternating bands from protomylonites to ultramylonites (Figure 5b, sample MD016), which contain dominantly top-NE kinematic indicators. The original compositional layering of the metasediments has strongly contributed to the amount of deformation and is associated with the formation of C-C′ shear band structures (Figure 5b). Microstructures indicate a strong dependency on the reactivation of the S1 foliation planes by repeated shearing and growth of chlorite. Increased amounts of strain are observed by the formation of ultramylonites, where S1 and S2 are (sub)parallel. The overall deformation is associated with lower grade metamorphic conditions observed by the replacement of epidote by chlorite, white mica (illite), and zoisite and continued growth of feldspar. In metasediments, this is observed by late-stage growth of chlorite. These observations indicate that the (retrograde) metamorphism in lower greenschist metamorphic facies took place at temperatures ~300°C, postdating the earlier phase of peak metamorphism.

3.3. D3 and D4 Contraction

The third deformation stage (D3) is observed both in the metamorphic core and in the surrounding nonmetamorphosed Mesozoic-Paleogene sediments and is characterized by upright and asymmetric folds with NNE-SSW trending fold axes (F3). D3 is associated locally with a widely spaced ESE dipping axial plane cleavage (S3) (Figure 6a). The folding is centimeter to meter scale and is particularly well observed in bedded sediments and schists and is accompanied by parasitic folding. The regional consistency of fold asymmetries

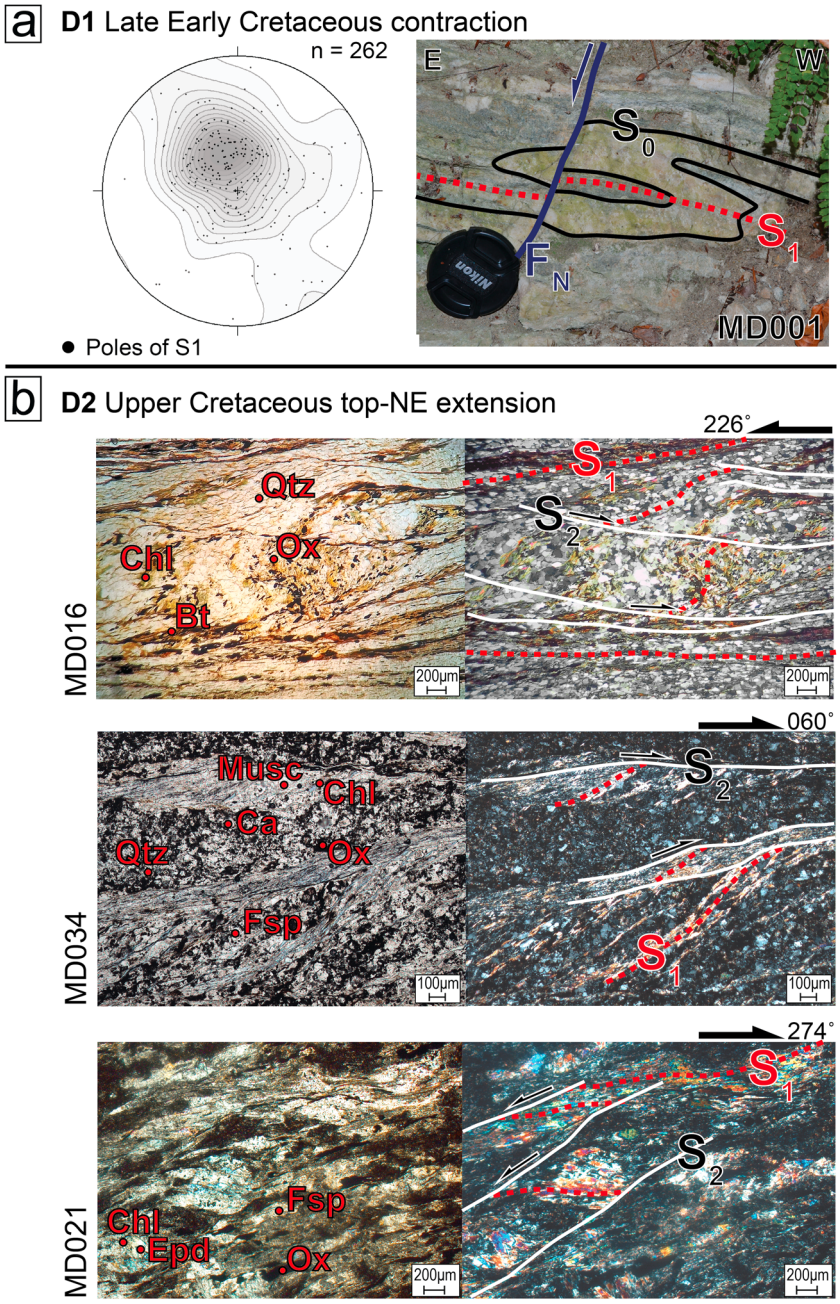

Figure 5. Examples of kinematic data, all locations are displayed in Figure 2. (a) Stereoplot of the poles to the S1 foliation projected over the contour plot of the data. Photo at locality *MD001* illustrates isoclinal folding (D1) of white marbles intercalated with tuffs, the S1 foliation, and a superposed normal fault (D5): fold axis 110/10, fault 073/35. (b) Thin-section photos illustrating the observed kinematics. Location *MD016*: plain polarized light (PPL) and cross-polarized light (XPL) photo of a mylonitic calc-schist with shear bands that indicate a top 046° (NE) sense of shearing. At the bottom of the picture, a zone of increased strain rate is present (ultramylonite) where S1 and S2 become parallel planes. The quartz in the thin section exhibits bulging as a result of dynamic recrystallization process during mylonitization. Location *MD034*: PPL and XPL photos of a greenschist indicating shearing of the S1 foliation along the S2 foliation with a top to 060° (ENE). The S2 foliation is amplified by renewed growth of chlorite. Location *MD021*: PPL and XPL of a metavolcanic with peak metamorphic mineral assemblage (e.g., epidote and feldspar) and overprinted by retrograde conditions (epidote is replaced by chlorite) during mylonitization. This sample is also used for Rb-Sr dating because the sample is located in the detachment. Sense of shear is top 094°, observed by the shearing of S1 along the S2 planes. Abbreviations: number of used data (n), bedding (S_0), normal fault (F_N) quartz (Qtz), chlorite (Chl), oxides (Ox), biotite (Bt), muscovite (Musc), calcite (Ca), feldspar (Fsp), epidote (Epd).

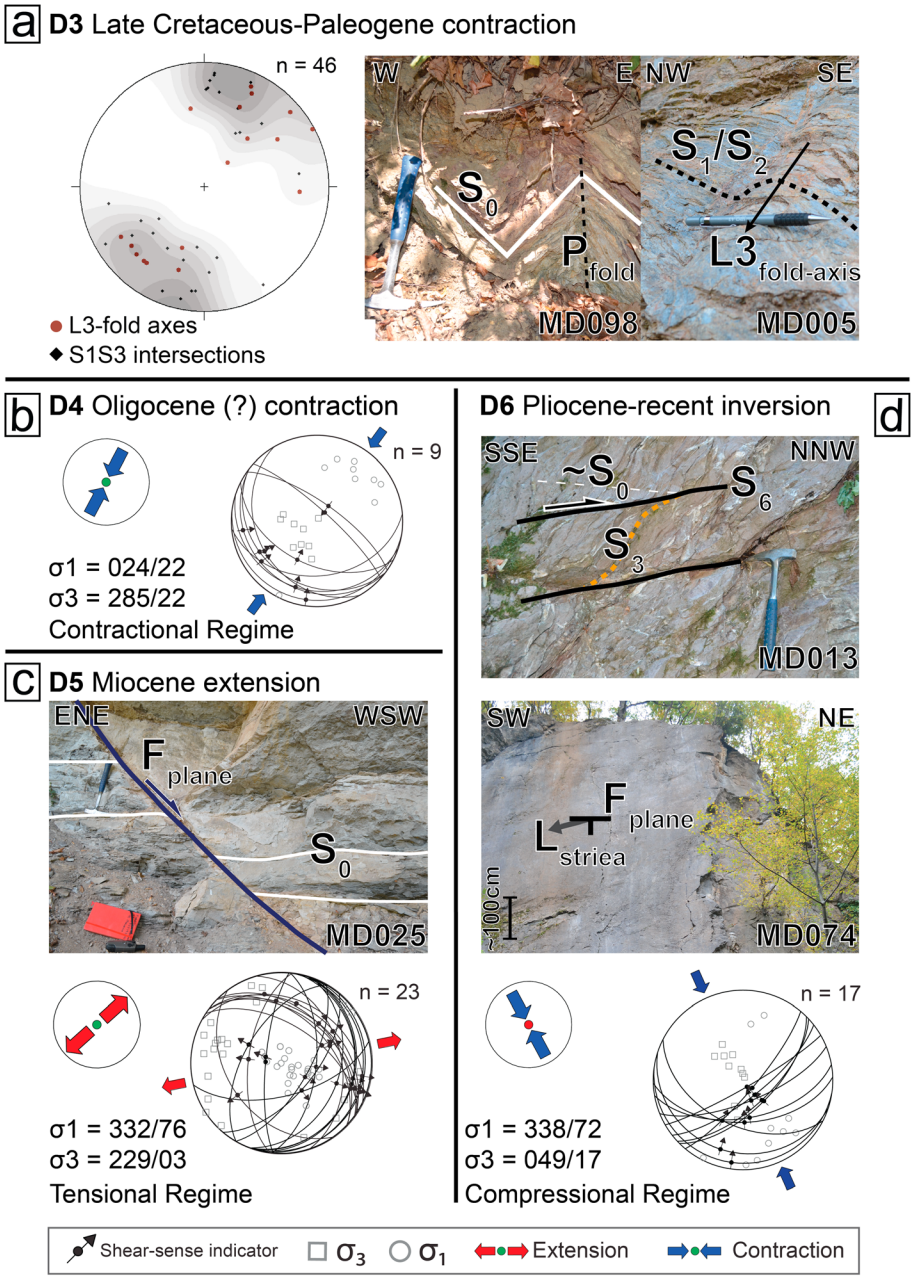

Figure 6. Examples of kinematic data; all locations are displayed in Figure 2. (a) Stereoplot of the L3 fold axes and the S1–S3 lines of intersection (where S1 is (sub)parallel to S2), projected on top of the contour plot. Mean strike of the fold axes is NE-SW. Photo of location *MD098* illustrates asymmetric folding of Upper Cretaceous siltic sandstones with fold axis 085/75. The photo at location *MD005* shows the mylonitic detachment with calc-schist of Triassic age. The S1 foliation is (sub) parallel to the mylonitic foliation (S2) with the position of the stretching lineation (L2) 234/10 and top 54 sense of shearing. The S1 and S2 are refolded by asymmetric folding during D3 contraction, fold axis 096/18. (b) Stereoplot of thrusts with NE vergence, such as the thrust in the SW part of the Medvednica Mountains emplacing Triassic deposits over Upper Cretaceous-Paleogene deformed sediments and paleostress tensor with the calculated direction of compression for the D4 deformation. (c) Example of normal faulting during the Miocene extension in location *MD025,* observed by decimeter offset of Miocene lacustrine sediments, fault plane 277/60. Stereoplot and associated paleostress tensor of normal faults that display an average top ENE sense of shear. (d) Location *MD013*: top-NW thrusting of deep-water Upper Cretaceous sediments during the post-Miocene inversion. The S3 cleavage planes are subsequently sheared during the S6 deformation: S6 position 130/50, bedding position 156/45. Location *MD074*: strike-slip fault, fault plane 210/70, striation 040/25, sinistral displacement. Stereoplot and associated stress tensor of the observed top-NW thrusts. Abbreviations: number of used data (n), foliation planes (S_1/S_2), bedding plane (S_0), fold plane (P_{fold}), fault plane (F_{plane}), striations (L_{striea}), fold axes D3 (L_3), principal stress directions (σ_1/σ_2).

suggests a top-WNW direction of tectonic transport. These folds affect sediments as young as the Paleocene and deform the tectonic contact between the metamorphic core and surrounding metamorphosed Mesozoic-Paleogene sediments. For instance, the asymmetric folding affects both the mylonitic calc-schists and the adjacent nonmetamorphosed black shales (e.g., location MD005, Figure 6a).

These contractional structures are affected by another set of NW-SE striking thrusts, dominantly dipping SW-ward (Figure 6b), that, although less frequently observed than D3 structures, are attributed to the next phase of shortening (D4). Particularly interesting are the outcrop structures observed in the vicinity of a large regional fault located in the SW part of the Medvednica Mountains (Figure 2, locations MD007, MD0095, and MD096). This fault places a shallow-marine Triassic sequence that includes Lower Triassic clastics, Middle and Upper Triassic biogenic limestones, and stromatolitic dolomites in its hanging wall over earlier folded Upper Cretaceous-Paleogene Gosau-type sediments in its footwall, which in turn is unconformably overlying Paleozoic weakly metamorphosed sequence. The significant thrust offset observed in the stratigraphy is accommodated by cataclastic deformation, particularly well developed in the Triassic limestones. Its kinematics, combined with structures observed in its vicinity, infers that this fault is a large thrust with SW direction of tectonic transport. At present, the fault dips in the same direction, most likely due its subsequent tilting.

3.4. D5: ENE Directed Extension

A prominent deformation feature of the entire Medvednica Mountains is the presence of normal faults in outcrops and at regional scale that are often associated with syntectonic deposition of Miocene sediments (D5). These normal faults are dominantly NW-SE to N-S striking and indicate a main top-ENE to top-NE direction of displacement (Figure 6c), although opposite WSW to W dipping faults are also observed in the field. Offsets range from decimeters (Figures 5a and 6c) to hundreds of meters, accommodated along zones of cataclastic deformation. Superposition criteria observed in the field indicate that this normal faulting postdates all previously described deformation events. One typical example shows that the folded mylonites at the contact between greenschist facies metamorphosed and subgreenschist facies Paleozoic or nonmetamorphosed units are crosscut by normal faults with ESE and NW directions of transport (location MD005, Figure 2). In more details, the normal faults change strike in map view, their orientations change from NW-SE in the NE part, where the largest offsets faults are documented, to NNE-SSW along the NW and SE flanks of the metamorphic dome (stereo plot in Figure 6c). There are no crosscutting relationships observed in the field between these normal faults; thus, their formation was likely coeval.

3.5. D6: Late-Stage Contraction and Strike-Slip Faulting

The last stage of deformation is a contractional event (D6) characterized by thrust faults dipping mainly south to SSE with top to the north to NNW transport direction (Figure 6d). In outcrops and at regional scale, these faults crosscut all previously described structures. For instance, D6 thrusting placed greenschist facies metamorphosed units over nonmetamorphosed Cretaceous deposits or the ophiolitic melange unit over Miocene and Pliocene deposits (Figure 9a). Locally, brittle shear bands are observed in the footwall of large thrusts (e.g., MD013, Figure 6d) by deformation appearing as a widely spaced cleavage (S6).

Thrusting is associated with a large number of local strike-slip faults (MD074, Figure 6d) possibly accommodating the lateral variations in shortening as tear faults. However, crosscutting relationships are unclear. In outcrops, the youngest deposits affected by this deformation are of Pliocene in age. Similar thrusts with up to 2 km offsets of the base Miocene horizon were observed along the northern margin of the Medvednica Mountains by the interpretation of reflection seismics [*Tomljenović and Csontos*, 2001], and further southeast in the Sava basin [*Ustaszewski et al.*, 2014]. The studies indicate that the thrusts presumably affected deposits as young as the Pliocene and Quaternary, as inferred by correlation of seismic lines with well data.

4. Thermochronology

According to our structural observations, the structural contact between the greenschist facies metamorphic core and the surrounding subgreenschist facies metamorphosed Paleozoic units and nonmetamorphosed Mesozoic sediments is the key characteristic of the Medvednica Mountains. Deriving the age of the ductile shear zone observed at this contact, as well as the timing of exhumation of the metamorphic core, is of critical

Table 1. Apatite and Zircon Fission Track Analytical Data[a]

	Lithology	Coordinates: Latitude	Coordinates: Longitude	Age (Ma ± 1σ)	$N_{Gr.}$	ρ_d ($\times 10^6$ cm^{-2})	N_d	ρ_s ($\times 10^6$ cm^{-2})	N_s	ρ_i ($\times 10^6$ cm^{-2})	N_i	P(χ^2) (%)	Disp.	MTL (μm ± SD_L)	N_L	Dpar
Apatite Fission Track																
MD-094	Gabbro (ophiolitic mélange)	45.91692	15.93919	17.3 ± 1.2	16	1.25	25,835	0.31	264	4.04	3,415	99.27	0.00	14.44 ± 1.04	16	3.33
Zircon Fission Track																
MD-093	Metakaratophyr (Triassic intrusive)	45.88778	15.96818	81.2 ± 7.3	7	0.50	15,508	7.49	482	2.94	189	99.89	0.00			
MD-094	Gabbro (ophiolitic mélange)	45.91692	15.93919	127.1 ± 8.1	14	0.50	15,508	7.64	1,466	1.91	366	98.63	0.00			
MD-101	Upper Cretaceous sandstone	45.87792	15.90892	126.5 ± 7.7	15	0.50	15,508	4.09	1,622	1.03	407	98.56	0.00			

[a]The presented ages are central ages with 1σ standard error [*Galbraith and Laslett*, 1993]. The data are discussed in the text, see also Figure 7. Abbreviations: $N_{Gr.}$ = number of dated apatite crystals; ρ_d = dosimeter track density; N_d = number of tracks counted on the dosimeter; ρ_d (ρ_i) = spontaneous (induced) track densities; N_s (N_i) = number of spontaneous (induced) tracks counted; P(χ^2) = probability of obtaining chi-square (χ^2) for *n* degrees of freedom (*n* is the number of crystals); Disp. = dispersion in single-grain ages; MTL = *C* axis projected mean track length with ± the standard deviation (SD_L); N_L = number of measured confined tracks; Dpar = average etch pit diameter.

importance for understanding the tectonic evolution of the NW part of the Internal Dinarides. A combination of low-temperature thermochronology and spatially controlled mineral Rb-Sr dating was used to reevaluate the relationship between the age of the structural contact and the timing of burial and subsequent exhumation.

Low-temperature thermochronology has been performed to derive cooling ages of the metamorphic core and those of the surrounding Paleozoic-Mesozoic units in the hanging wall of the structural contact. We have analyzed samples for zircon fission track (ZFT) and apatite fission track (AFT) dating, targeting the cooling trajectory below 250°C. Combining AFT and ZFT allows reconstructing the cooling trajectory for the Medvednica Mountains, and thereby shedding light on the different tectonic processes that occurred in the NW Internal Dinarides.

The spatially controlled Rb-Sr dating was performed to constrain the age of metamorphic events, mylonitic fabrics, and associated deformation. Key sample locations were chosen to date these processes, with samples taken from the center of the greenschist facies metamorphic core and from the mylonitic zone located at its margin.

4.1. Apatite and Zircon Fission Track Dating

Zircons and apatites are fairly rare in the sampled lithologies of the metamorphic core, which is dominated by basic metavolcanics and metasediments (shallow- or deep-water limestones). Moreover, other more suitable lithologies were not available in the field due to outcrop scarcity. A total of seven samples were analyzed for AFT and ZFT dating. Three samples (Figure 2, MD005, MD093, and MD102) were taken from the greenschist facies metamorphic core, including two samples from the metavolcanics (MD005 and MD093) and a metasediment (MD102). The other four samples (Figure 2, MD094, MD101, MD109, and MD113) were collected from the nonmetamorphosed units: sample MD094 is a gabbro from the ophiolitic mélange, MD101 a sandstone from the Cretaceous flysch, MD109 a Paleozoic (meta)sandstone, and MD113 a Lower Triassic sandstone. From the seven samples, only three samples contained zircons suitable to perform fission track analysis, i.e., MD093, MD094, and MD101. Only one sample (MD094) contained enough apatites for fission track analysis. ZFT and AFT analytical results are presented in Table 1.

The extraction of apatites and zircons from the rock samples (4–5 kg per sample) was performed by a standard mineral separation procedure [e.g.,

Table 2. Analytical Data of the Rb-Sr Thermochronology[a]

Sample code	Lithology	Phase	Rb	Sr	Rb/Sr	$^{87}Rb/^{86}Sr$	$^{87}Sr/^{86}Sr$	Sr/Sr (SE%)
MD-021	Metakaratophyr (Triassic intrusive)	Whole Rock	18.533	220.259	0.084	0.2419	0.7062	0.0012
		Epidote	25.331	2133.613	0.012	0.0343	0.7059	0.0008
MD-029	Calc-schist (Triassic protolith)	Whole Rock	72.293	185.616	0.389	1.1201	0.7086	0.0011
		Calcite	3.650	415.592	0.009	0.0253	0.7069	0.0011
MD-064	Upper Cretaceous sandstone	Whole Rock	104.872	41.234	2.543	7.3341	0.7364	0.0010
		Biotite	72.066	19.211	3.751	10.8231	0.7418	0.0049
		Chlorite	12.006	450.445	0.027	0.0770	0.7250	0.0013

[a]The description of the data is discussed in the text, see also Figure 8.

Merten, 2011] at VU University Amsterdam (Netherlands). Following the mineral separation, zircon and apatite concentrates were prepared for irradiation. This includes mounting, grinding, polishing, and etching of the apatite and zircon crystals. The etched mounts are attached against an external detector [*Gleadow*, 1981; *Gleadow and Lovering*, 1977] and subsequently irradiated at the nuclear reactor in Munich. During irradiation, the neutron flux is monitored with a CN5 dosimeter glass for the apatite mounts and a CN1 dosimeter glass for the zircon mounts. Additional information on the AFT and ZFT analytical procedures can be found in *Reiners and Ehlers* [2005] and references therein.

After irradiation, the numbers of tracks in the apatites, zircons, and external detectors were counted, accompanied by the measurement of apatite fission track lengths. With these data, the ages were calculated using the Trackkey software, version 4.2 by *Dunkl* [2002]. To calculate the ages, the zeta calibration method [*Hurford and Green*, 1983] was used with a zeta factor of 352 ± 10 for the CN5 glass (apatites) and 128 ± 3 for the CN1 glass (zircons). To analyze the homogeneity of the single-grain ages per sample, the chi-square (χ^2) test was used, which returns the probability ($P(\chi^2)$) that the single-grain ages are derived from the same population. When a $P(\chi^2) > 5\%$ is obtained, the sample passes the chi-square test, and therefore, the age population can be considered to be homogeneous [*Barbarand et al.*, 2003; *Bernet*, 2009].

Finally, to constrain the cooling trajectories for the Medvednica Mountains, the AFT cooling ages and AFT length data were combined and modeled using inverse modeling in the HeFTy software. This software is based on fission track annealing algorithms [*Ketcham*, 2005; *Ketcham et al.*, 2007].

4.2. Rb-Sr Chronology

Spatially controlled mineral isochrons [e.g., *Muller*, 2003] were obtained on four samples. The four samples (Figure 2, MD021, MD029, MD050, and MD064) were collected in the vicinity of the detachment, as defined by the mylonitic zone between the greenschist facies metamorphic core and subgreenschist facies to nonmetamorphic units. Two of the selected samples (MD021 and MD050) are metavolcanics with a mylonitic fabric, while sample MD029 is a metasediment and the sample MD064 is Paleozoic sandstone with minor recrystallization. Rb-Sr results are presented in Table 2.

The isotopic ratios of $^{87}Sr/^{86}Sr$ and the trace element concentrations of Rb and Sr were measured by thermal ionization mass spectrometry on whole rock or mineral separate fractions. Whole-rock samples were crushed to about one third of their grain size. Mineral fractions were obtained by microsampling of thin sections or their billets using a Micromill [*Ducea et al.*, 2003]. Powders were put in large Savillex vials and dissolved in mixtures of hot concentrated HF-HNO_3 or, alternatively, mixtures of cold concentrated HF-$HClO_4$. The dissolved samples were spiked with the Caltech Rb and Sr spikes [*Ducea and Saleeby*, 1998]. After dissolution, the Rb and Sr were separated in cation columns containing AG50W-X4 resin, using 1 N to 4 N HCl. Rb was loaded onto single Re filaments using silica gel and H_3PO_4. Sr was loaded onto single Ta filaments with Ta_2O_5 powder.

Mass spectrometric analyses were carried out at the University of Arizona on an automated VG Sector multicollector instrument fitted with adjustable Faraday collectors and a Daly photomultiplier [*Otamendi et al.*, 2009]. Concentrations of Rb and Sr were determined by isotope dilution, with isotopic compositions determined on the same spiked runs. An off-line manipulation program was used for isotope dilution calculations. Typical runs consisted of acquisition of 100 isotopic ratios. The mean result of 10 analyses of the standard NRbAAA performed during the course of this study is $^{85}Rb/^{87}Rb = 2.61199 \pm 20$. Fifteen analyses of standard

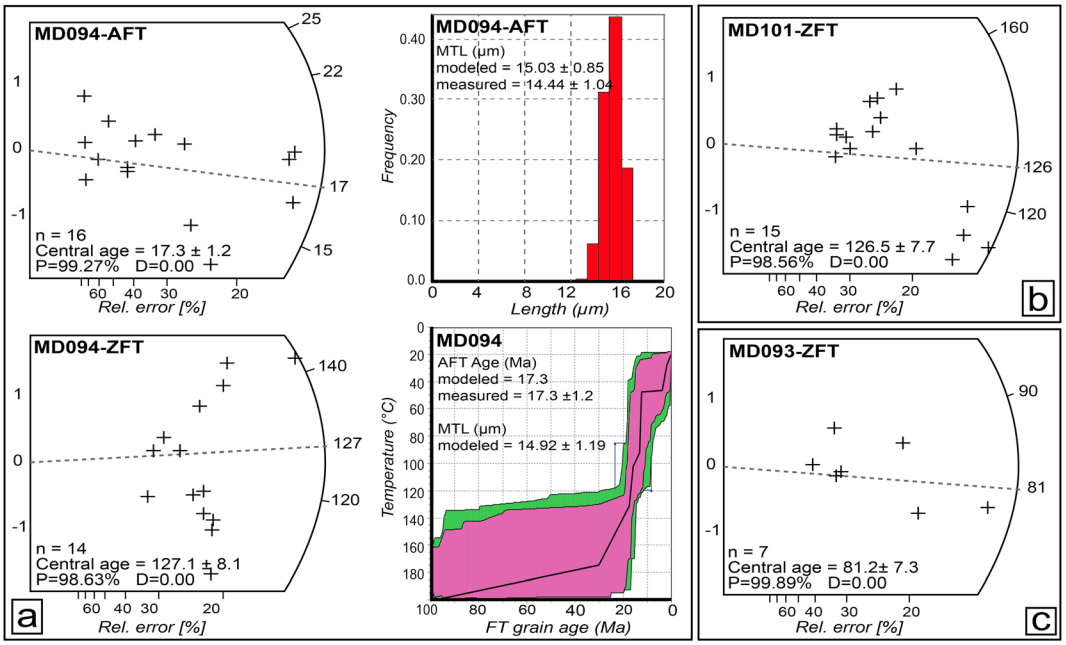

Figure 7. Fission track data. (a) Radial plots showing the distribution of cooling ages according to the relative error and standard deviation for the apatites (upper plot) and zircons (lower plot) in sample MD094, accompanied by a graph showing the distribution of the track lengths in the apatites for sample MD094 (upper right graph) and a graph illustrating the HeFTy modeling results (lower right graph) based on track length and age distribution of the apatite fission tracks. The HeFTy model suggests accelerated Miocene cooling. (b) Radial plot showing the distribution for the measured zircon fission track cooling ages in sample *MD101* located in the hanging wall of the detachment. (c) Radial plot showing the distribution for the measured zircon fission track cooling ages in sample *MD093*, located in the footwall of the detachment. Abbreviations: number of used data (n), probability (P), dispersion in single-grain ages (D), mean track length (MTL). Location of all samples is displayed in Figure 2.

Sr_{987} yielded mean ratios of $^{87}Sr/^{86}Sr = 0.710285 \pm 7$ and $^{84}Sr/^{86}Sr = 0.056316 \pm 12$. The Sr isotopic ratios of standards and samples were normalized to $^{86}Sr/^{88}Sr = 0.1194$. The estimated analytical $\pm 2\sigma$ uncertainties for samples analyzed in this study are $^{87}Rb/^{86}Sr = 0.35\%$ and $^{87}Sr/^{86}Sr = 0.0014\%$, and procedural blanks averaged from five determinations were Rb 10 pg and Sr 150 pg.

4.3. Fission Track Results

Three samples with suitable zircons yielded results. Samples that were collected in places situated outside the greenschist facies metamorphic core yield a central age of 127.1 ± 8.1 Ma for MD094 and 126.5 ± 7.7 Ma for MD101 (Figures 7a and 7b). Both samples pass the chi-square test with values above 5% (Table 1). The depositional age of the gabbro sample MD094 from the ophiolitic mélange is Jurassic (an ophiolitic block in the ophiolitic melange of Jurassic to presumably Earliest Cretaceous age [*Babić et al.*, 2002]), and the depositional age of the detrital sample MD101 is Late Cretaceous (Campanian Gosau-type deposits). The depositional ages suggest that the obtained ZFT age for sample MD094 is related to postdepositional cooling subsequent to burial, e.g., in response to orogenic buildup. However, sample MD101 most likely represents a cooling age of a sediment source area because the obtained cooling age is older than the depositional age. Furthermore, these two samples are in close proximity and are almost identical with respect to their cooling ages, suggesting a high possibility that the source area of the Late Cretaceous sample MD101 is the neighboring ophiolitic mélange. This implies a very short sediment transport and is in agreement with the observation of Jurassic-Lowermost Cretaceous ophiolitic mélange detritus found in the Upper Cretaceous sediments.

Sample MD093 is a metavolcanic sample taken from the greenschist facies metamorphic core that has a ZFT central age of 81.2 ± 7.3 Ma and passed the chi-square test (Figure 7c). The age suggests significant Late Cretaceous cooling of the metamorphic core that postdates the late Early Cretaceous metamorphism.

Only one single AFT sample contained sufficient apatites, sample MD094, which is the same gabbro from the ophiolitic mélange as described above. This yields an AFT central age of 17.3 ± 1.2 Ma and a measured mean track length of 14.44 ± 1.03 μm (Figure 7a). The ZFT age, the AFT age, and length measurements combined with metamorphic and stratigraphic constraints were used to derive the cooling trajectory of sample MD094 by using the HeFTy software. The age-temperature model (Figure 7b) indicates that the units outside the greenschist facies metamorphic core have remained at high-temperature conditions until Miocene times. The long length of the apatite fission tracks, 15.03 ± 1.24 μm when corrected for the angle of measurement, suggests that the sample must have passed rapidly through the partial annealing zone. The HeFTy model suggests a temperature drop from 140°C to 50°C between 20 and 15 Ma. The observed cooling rate is in the order of 18°C/Ma compatible with denudation rates in the order of 0.7 km/Ma, when assuming an average thermal gradient of 25°C/km.

In summary, the ZFT and AFT data indicate multiple cooling phases. ZFT ages indicate a Lower Cretaceous (Barremian-Aptian) cooling age of the areas presently situated outside the greenschist facies metamorphic core as well as the source area shedding the uppermost Cretaceous sediments. In contrast, the metamorphic core cooled below ~240°C during the Late Cretaceous. The only AFT age obtained for sample MD094 located outside the greenschist facies metamorphic core indicates rapid Miocene cooling.

4.4. Rb-Sr Dating Results

Rb-Sr chronology typically has closure temperatures in a range of 300–500°C [*Muller*, 2003] although for most minerals diffusion data are sparse and are influenced by grain size or cooling rates. Biotite, for example, has a Rb-Sr closure temperature of around 280–320°C in equilibrium with a pelitic whole rock [*Dodson*, 1973]. Despite uncertainties in closure temperatures, the technique is successfully applied to low-grade metamorphism in extensional systems, in cases where those rocks did not undergo subsequent metamorphism in a later orogenic cycle. Since cooling through that temperature range (300–500°C) is fast in extensional systems, most pairs of mineral-whole rocks found in low-grade rocks subject to mylonitization and newly forming minerals in extensional systems (with common minerals being calcite, epidote, chlorite, or biotite) will record the timing of that fast event spanning the brittle-ductile transition temperature range.

Rb-Sr chronology was performed in this study on four samples (MD021, MD029, MD050, and MD064) using whole rock and various individual minerals (Table 2). Isochrons [*Ludwig*, 2012] were obtained for samples MD021, MD029, and MD064 (Figure 8), but not for MD050. The MD021 isochron uses epidote and whole-rock fractions and has an age of 110.2 ± 3.0 Ma. The MD029 isochron was determined using whole rock and calcite fractions and has an age of 113.4 ± 0.7 Ma. For the MD064, we use chlorite, biotite, and the whole-rock fractions, which define an isochron corresponding to an age of 110 Ma ± 22 Ma.

5. Interpretation: Integrated Structural and Thermochronological Data

All previous studies of the Medvednica Mountains assumed that the subgreenschist facies Paleozoic metasediments, largely outcropping in the W/NW and NE, together with the greenschist facies metamorphosed Paleozoic-Triassic volcanics and sediments are both part of the same tectonic unit, i.e., the Medvednica metamorphic complex [e.g., *Tomljenović et al.*, 2008, and references therein]. However, the subgreenschist facies Paleozoic metasediments have experienced only low-grade metamorphism with peak temperatures of 100–240°C [*Judik et al.*, 2006] when compared with the peak temperatures of the greenschist facies part of the metamorphic complex in the order of 350–410°C. Our structural analysis shows that these two rock units characterized by different metamorphic grades are part of two different tectonic units that are separated by a major shear zone (Figure 9). The analysis of the tectonic unit situated in its hanging wall demonstrates that the first deformation and very low degree metamorphism of the Paleozoic rocks must be (late) Variscan, subsequently unconformably overlain by Mesozoic nonmetamorphosed sediments. This is in contrast with the Early Cretaceous age of the greenschist facies metamorphism of the Paleozoic-Triassic volcanics and sediments that are part of another tectonic unit situated in the footwall of this shear zone. Some reheating occurred at the base of the higher tectonic unit during the late Early Cretaceous burial, as observed in Paleozoic rocks by *Judik et al.* [2008], but at significantly lower metamorphic conditions (i.e., subgreenschist facies) when compared with the greenschist facies of the lower tectonic unit. Therefore, we further make a clear distinction between these two tectonic units (Figure 9).

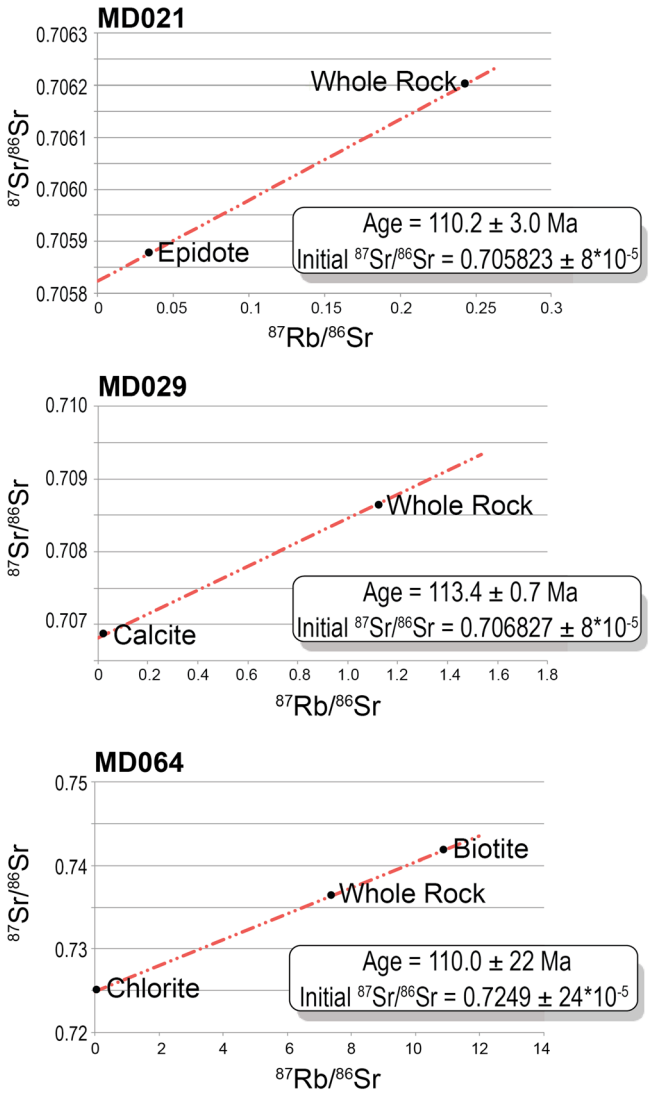

Figure 8. Rb-Sr isochron graphs for the samples MD021, MD029, and MD064. The errors shown for the sample ages are twice the standard deviation. The sample locations are displayed in Figure 2, and sample description is further described in the text.

5.1. Cretaceous Kinematics and Tectonothermal Evolution

Convergence between Adria and Europe continued in the Dinarides after the Middle Jurassic to earliest Cretaceous obduction of ophiolites over the distal Adriatic passive margin [e.g., *Schmid et al.*, 2008]. In the area of the Medvednica Mountains, this continuation resulted in a late Early Cretaceous event of nappe stacking, burial, and metamorphism in greenschist facies of the Paleozoic-Triassic volcanics and sediments of the lower tectonic unit (Figures 3 and 9). In this unit, the nappe stacking correlates with our D1 phase of deformation associated with coaxial flattening, isoclinal folding, and greenschist facies metamorphism with peak temperatures up to ~400°C. The Rb-Sr age dating indicates that metamorphism occurred between 135 and 110 Ma, in agreement with previous studies [e.g., *Borojević Šostarić et al.*, 2012, and references therein]. The contraction direction (NW-SE) of our study is in agreement with previous structural studies of the Medvednica Mountains [e.g., *Tomljenović et al.*, 2008]. By correcting for the Late Paleogene-Early Miocene 130° clockwise rotations and the 30° Miocene-recent counterclockwise rotations of the Medvednica Mountains [*Tomljenović et al.*, 2008], the original contraction would be NE-SW oriented. A NE-SW directed contraction is commonly observed in the Dinarides, but at later times, during the Late Cretaceous-Eocene [e.g., *Tari-Kovačić and Mrinjek*, 1994; *Schmid et al.*, 2008, and references therein]. In the upper tectonic unit, the deposition of Aptian-Cenomanian shallow-marine and near-shore flexural basin sequence that unconformably overlays the Paleozoic-Mesozoic and ophiolitic mélange units [*Lužar-Oberiter et al.*, 2012] can be interpreted as synkinematic deposition to the late Early Cretaceous thrusting.

This initial nappe stack was overprinted by a D2 top-NE Late Cretaceous event that created pervasive mylonitization and NE plunging stretching lineations in the greenschist facies metamorphic core (D2). In this lower unit, a second stage of lower greenschist facies metamorphism under retrograde conditions took place during D2 shearing, observed mostly by the breakdown of epidote and renewed growth of chlorite and feldspar. This shearing and retrograde metamorphism is particularly concentrated at the structural contact between the two tectonic units and decreases at farther distances in the greenschist facies metamorphic core. Based on the available structural data, we interpret D2 as an expression of NE-directed extension that reactivated the earlier late Early Cretaceous nappe contact as a major detachment. This reactivation was facilitated by the presence of metamorphosed carbonate material (marbles and calc-schists) in the upper part of the greenschist facies metamorphic core that resulted in the formation of calc-mylonites. The presence of such

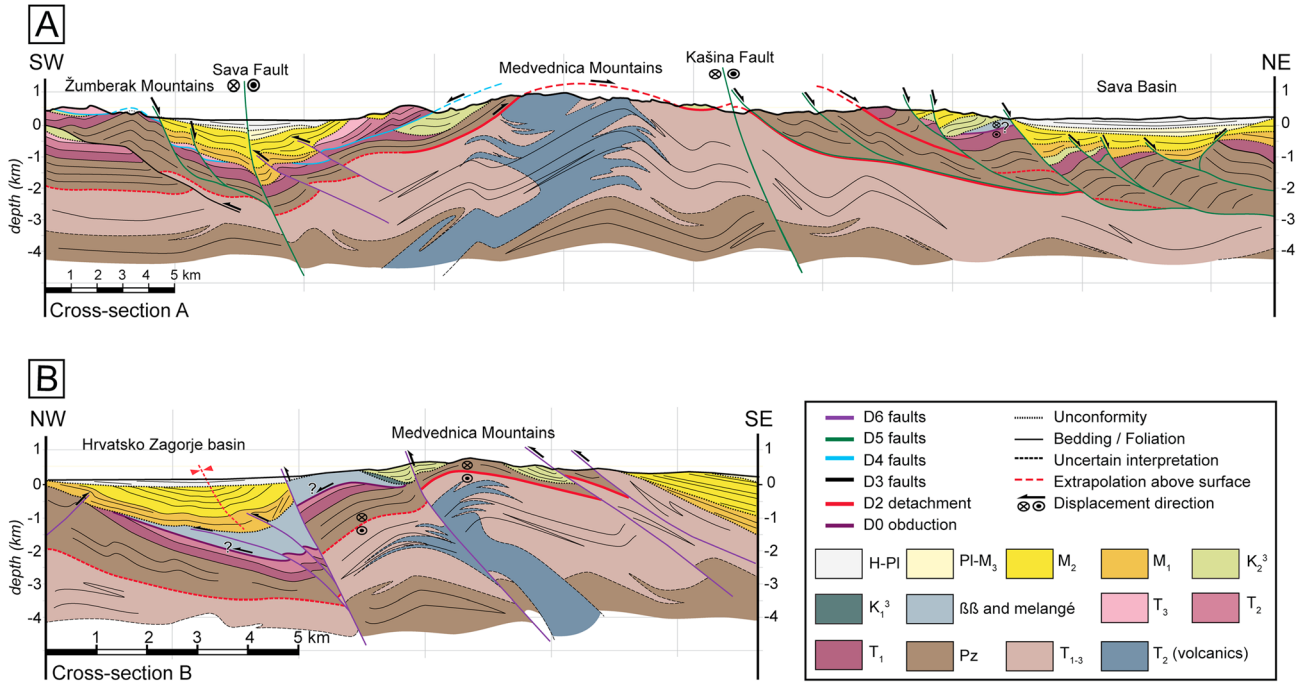

Figure 9. Cross sections across the Medvednica Mountain. (a) NE-SW oriented section and (b) NW-SE oriented section. Note the slight vertical exaggeration of the profiles. The location of cross sections is displayed in Figures 1b, 2, and 4. Abbreviations: Upper Paleozoic (Pz), Lower Triassic (T_1), Middle Triassic (T_2), Upper Triassic (T_3), metamorphosed Triassic (T_{1-3}), ophiolite (ββ), Lower Cretaceous (Aptian-Cenomanian) (K_1^3), Upper Cretaceous (Senomanian) (K_2^3), Lower Miocene (M_1), Middle Miocene (M_2), Pliocene-Upper Miocene (Pl-M_3), Quaternary (Q).

rocks at temperatures in excess of 300°C creates rheological weak zones that focus deformation [*Schmid et al.*, 1977]. Reactivation of inherited nappe contacts as extensional detachments due to the presence of rheological weak layers consisting of metamorphosed carbonatic cover, ophiolitic mélanges, or turbidites in the upper part of buried nappes is commonly observed in the Internal Dinarides [*Matenco and Radivojević*, 2012; *Schefer et al.*, 2011; *Stojadinović et al.*, 2013; *Toljić et al.*, 2013; *Ustaszewski et al.*, 2010]. The formation of the detachment was associated with the onset of Upper Cretaceous deposition in the hanging-wall unit. This deposition shows clear syndepositional normal faulting with the same top-NE transport direction. It also has the typical hanging-wall extension initiation characteristics of an overall transgression with coarse continental fan lobes in the proximity of the detachment passing laterally and upward to alluvial fans, proximal marine, and continental shelf deposits, and ultimately to deep-water sedimentation. The initial continental deposition is interpreted as a rift initiation type of sedimentation [sensu *Prosser*, 1993]. Therefore, we interpret the activation of the extension and the formation of the top-NE detachment to be coeval with the initiation of the Upper Cretaceous sedimentation in the hanging wall of the detachment. This is confirmed by the single ZFT age obtained in the lower tectonic unit of the greenschist facies metamorphic core that indicates a cooling age of ~81 Ma, interpreted as an extensional exhumation of the footwall unit.

The detachment was responsible for the tectonic omission observed in the jump of metamorphic degree between the two tectonic units (Figure 9). This is evident even when comparing the metamorphic degree of the greenschist facies footwall with the subgreenschist facies Paleozoic sediments of the hanging wall (Figure 9). Farther to the NE, this deformation created a second weakly mylonitic to cataclastic top-NE shear zone that juxtaposed Middle Triassic rocks in its hanging wall in contact with Paleozoic metasediments in the footwall (Figure 9a). Its geometry and smaller tectonic omission suggest that this is an excisement splay formed during the late stages of exhumation. Restoring the post-Eocene clockwise and subsequent counterclockwise paleomagnetic rotations imply that the presently observed top-NE sense of shear along the detachment was originally top NW at the time of deformation.

5.2. Latest Cretaceous to Neogene Tectonic Evolution

The Late Cretaceous extension was subsequently followed by shortening that created NW verging thrusts and folds in their present-day orientation (D3). In agreement with previous studies [*Tomljenović et al.*, 2008], we interpret these structures to be formed during the latest Cretaceous-Eocene phases of Dinaridic collision. Deformation started during the latest Cretaceous, most likely Maastrichtian, with the deposition of syncontractional turbidites that continued the deep-water deposition of the earlier synextensional and postextensional sediments. All these sediments were deformed together with the overlying Paleocene deposits. This deformation correlates with the typical latest Cretaceous and Eocene stages of shortening observed throughout the Dinarides, which took place during the collision between Europe and Adria [*Dimitrijević*, 1997; *Schmid et al.*, 2008; *Ustaszewski et al.*, 2010]. Our observations were unable to differentiate two separate stages of contraction (i.e., latest Cretaceous and Eocene) as inferred elsewhere, although such a differentiation may emerge in further studies. Taking into account the post-Eocene clockwise and subsequent counterclockwise rotations [*Tomljenović et al.*, 2008], the presently NW verging D3 structures would be SW verging at the time of deformation, which is a typical and coeval Dinaridic vergence.

A new stage of contraction followed (D4) that was characterized by NE-SW oriented shortening in present-day orientation. This stage is marked in particular by the out-of-sequence emplacement of the Žumberak nappe [*Tomljenović et al.*, 2008] in the SW part of our study area. Here Triassic shallow-marine clastics and carbonates are thrusted over the subgreenschist facies Paleozoic metasediments and Upper Cretaceous-Paleogene deposits (Figure 2). In contrast to previous studies, we infer that the transport direction is top SW in its present-day orientation (Figure 9a) based on limited available field kinematic indicators. To the SW of the studied area in Žumberak Mountains (Figure 1b), the Žumberak nappe thrusts mainly Upper Triassic dolomites, similar in facies to the Carnian-Norian Hauptdolomit (or Dolomia Principale) of the Southern Alps, over an ophiolitic mélange and Cretaceous-Paleogene sediments (Figure 1b) [*Tomljenović*, 2002]. Interestingly, the Upper Triassic shallow-water facies of the Žumberak nappe contrasts with coeval deep-water facies documented in the internal part of the Dinarides following the overall deepening of the Adriatic passive continental margin [e.g., *Dimitrijević*, 1997; *Starijaš et al.*, 2010; *Toljić et al.*, 2013]. Thus, when compared with the facies of typical internal Dinaridic nappes, which include the Medvednica Mountains [see *Schmid et al.*, 2008], the paleogeographic provenance of the Žumberak nappe is different. The emplacement age of the Žumberak nappe must be sometimes during the Oligocene-earliest Miocene, postdating the Late Cretaceous-Eocene shortening (D3) and predating the Miocene extension of the Pannonian Basin. Given the coeval large-scale clockwise and subsequent counterclockwise rotations of the Medvednica Mountains, it is difficult to reconstruct the sense of shear at the times of Žumberak nappe emplacement, but it could have been somewhere between top south to top SE at the time of deformation.

The extension of the Pannonian Basin starting at ~20 Ma is well documented in the larger region of the Medvednica Mountains [*Fodor et al.*, 2008; *Horváth et al.*, 2006; *Ustaszewski et al.*, 2010]. It affected both the Medvednica Mountains, by formation of normal faults as documented in our study (D5, Figure 9a) and by seismic interpretation in the neighboring Sava and Drava basins [*Tomljenović and Csontos*, 2001; *Saftić et al.*, 2003; *Ustaszewski et al.*, 2014]. Furthermore, the normal faulting is dominantly of low angle and listric in geometry, the coeval Miocene sedimentation in the hanging wall being associated with footwall erosion (Figure 9a). This demonstrates that the extension was asymmetric and was associated with gradual exhumation of the Medvednica Mountains in the footwall of normal faults or brittle detachments. This is in agreement with our single AFT age and the thermal modeling, which suggests enhanced cooling between 20 and 15 Ma (Figure 7a) interpreted as tectonic exhumation. Furthermore, the extension has reactivated the Late Cretaceous detachment as inferred by cataclastic deformation overprinting the mylonites at the contacts of the greenschist facies metamorphic core with the Miocene sediments. The Miocene exhumation of the Medvednica Mountains has resulted in a dome-like geometry with the dominant top NE to ENE sense of transport and deviations toward NE-SW oriented near the NW and SE margins (Figures 2 and 6c). Such a geometry and kinematics of normal faults suggests exhumation during extension and is often observed in other core complexes or brittle detachments that have a dome-like geometry [e.g., *Jolivet et al.*, 2004; *Lister and Davies*, 1989; *Matenco and Schmid*, 1999].

The last stage of deformation (D6) observed by our data is a post-Miocene top-NW thrusting (Figure 9b). This deformation is in agreement with previous field kinematic and morphological studies in the Medvednica Mountains and with seismic interpretations of the surrounding area, e.g., the Sava basin [*Matoš et al.*, 2014;

Saftić et al., 2003; *Tomljenović and Csontos*, 2001; *Tomljenović et al.*, 2008; *Ustaszewski et al.*, 2014]. As proposed by *Tomljenović and Csontos* [2001], this shortening took place in response to the coeval northward convergence and counterclockwise rotation of Adria in respect to Europe [see also *Bada et al.*, 2007; *Vrabec and Fodor*, 2005], which started at around 7 Ma in the larger area of the Southern Pannonian Basin [*Uhrin et al.*, 2009; *Matenco and Radivojević*, 2012].

6. Discussion

Our study demonstrates that the area of Medvednica Mountains in NW Croatia was affected by a complex polyphase tectonic history including multiple events of thrusting and nappe stacking interrupted by two periods of extensional deformation and associated exhumation. A special remark is reserved for the late Early Cretaceous nappe stacking and burial of the metamorphic core to greenschist facies conditions. Although documented previously [e.g., *Pamić*, 1993], this deformation event has yet no clear explanation in the overall context of Dinarides tectonic evolution. Outside the study area, this contraction is documented by the formation of a regional unconformity postdating the late Jurassic-Earliest Cretaceous obduction of Western Vardar unit, observed for instance in the pre-karst or Drina-Ivanjica units of Montenegro and Serbia [*Schmid et al.*, 2008]. Farther to the SE in the prolongation of the Dinaridic units, this event is responsible for large-scale thrusting and metamorphism up to amphibolitic facies of the Pelagonian units of the Hellenides [*Kilias*, 2010 and references therein]. Closer to our studied area, coeval or postdating deformation took place in the well-known Austroalpine nappe stack of the Eastern Alps that resulted in large-scale contraction and metamorphism [e.g., *Neubauer et al.*, 1995, and references therein]. We suggest that the kinematics and timing of the late Early Cretaceous deformation in the Medvednica Mountains is better correlated with the latter area. The reconstructed NE-SW direction of the late Early Cretaceous shortening cannot be directly correlated with the postdating latest Cretaceous-Eocene contraction in the Dinarides because these are two different tectonic events separated by the Late Cretaceous extension and not just one continuous process.

6.1. Late Cretaceous Extensional Exhumation

The formation of an extensional detachment during Late Cretaceous times at around 80 Ma explains the tectonic omission observed in the Medvednica Mountains between the greenschist facies metamorphic core and surrounding Paleozoic-Triassic sediments. Besides the presented field evidence, this new interpretation is based on a compilation of previously published thermochronological data (Figure 10). Vitrinite reflectance data and Ar/Ar white mica ages from the metamorphic core indicate temperatures in the order of 300–410°C during the Early Cretaceous. In contrast, vitrinite reflectance data and K/Ar illite ages indicate temperatures in the order of 200–230°C in the hanging wall of the metamorphic core for the same period of time (Figure 10). The inclusion of our new data added in this compilation allowed for a precise correlation of the time-temperature paths in the footwall and hanging-wall units and thus provides critical constraints on the timing of the tectonic omission. The Rb-Sr isochron ages between 110 and 113 Ma are important in specifying the time-temperature history in the greenschist facies metamorphic core during Early Cretaceous times (Figure 10). Extensional exhumation of the lower unit constrained by the Upper Cretaceous synkinematic sedimentation and a single ZFT age of ~81 Ma (Figure 7c) is a robust feature. The Early Cretaceous ZFT cooling and provenance ages (126–127 Ma) obtained from outside the greenschist facies metamorphic core increased the precision of the time-temperature curve in the same range detected by previous studies (Figure 10). The short-range sediment transport of Jurassic-Earliest Cretaceous ophiolitic mélange detritus deposited in Upper Cretaceous sediments is in agreement with previous provenance studies [*Lužar-Oberiter et al.*, 2012].

Similar Late Cretaceous exhumation of dome-shaped metamorphic cores in the footwall of major detachments is a characteristic feature of the neighboring Eastern Alps [e.g., *Froitzheim et al.*, 1997; *Neubauer et al.*, 1995]. For instance, the Late Cretaceous Gleinalm dome [e.g., *Neubauer et al.*, 1995] has reactivated an inherited nappe contact and exhumed a metamorphic nappe stack along a low-angle detachment separating amphibolite-grade rocks in the footwall from Paleozoic lower greenschist facies rocks in the hanging wall. Along this structure, the footwall accommodated a significant amount of vertical thinning associated with noncoaxial shear, while the hanging-wall recorded the synkinematic deposition of Upper Cretaceous Gosau sediments. These sediments were deposited in basins formed on top of a thickened and metamorphosed crust and contain Middle Santonian continental to lacustrine deposits followed by Campanian deep-marine sediments. Basin

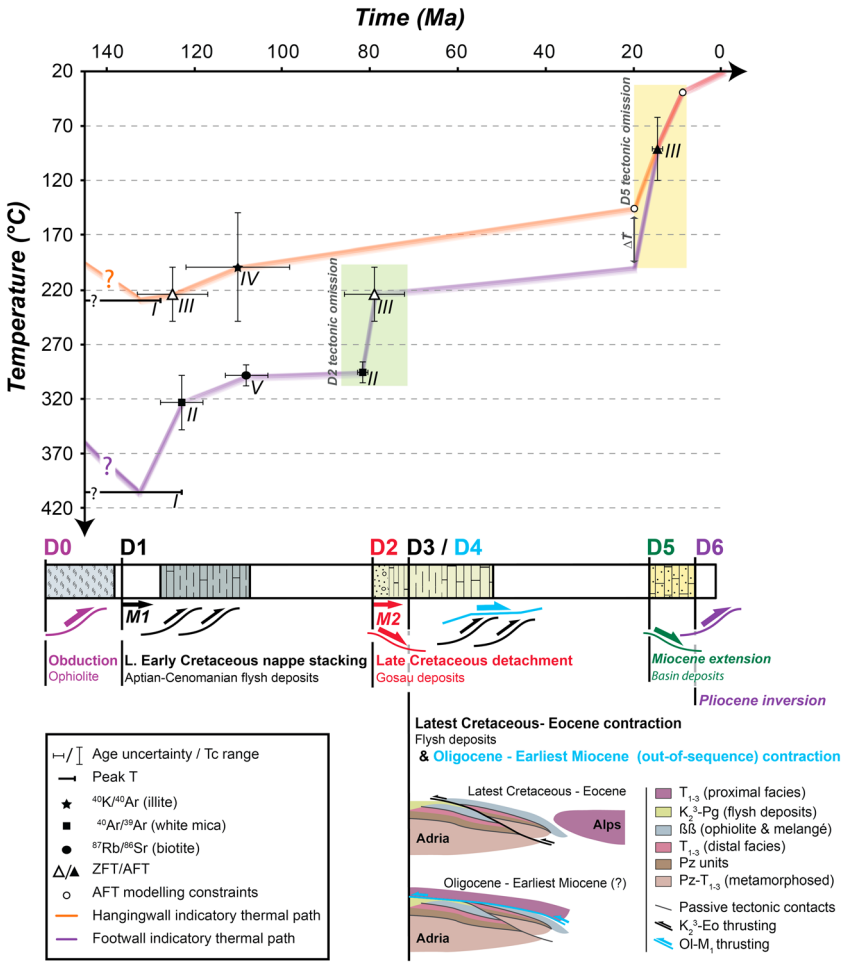

Figure 10. A temperature-time graph illustrating the thermal evolution of the hanging wall versus the footwall of the detachment, and their position in time compared to the tectonic, metamorphic, and sedimentary events. Geochronological data and their error bars compiled from I *Judik et al.* [2008], II *Borojević Šostarić et al.* [2012], III this study, IV *Judik et al.* [2006] and *Belak et al.* [1995], and V this study. The thermal paths for the hanging wall and footwall join the mean age and mean closure temperature for each data point. Therefore, the lines are in the center of the error bars. For the abbreviations, see the figure caption of Figure 9.

subsidence was coeval with the exhumation of metamorphic basement along low-angle detachments within an overall tectonic setting characterized by N-S convergence and E-W extension [*Froitzheim et al.*, 1997; *Fügenschuh et al.*, 2000; *Neubauer et al.*, 1995; *Willingshofer et al.*, 1999a]. The extensional exhumation of the metamorphic basement and the subsidence of the Gosau basins in the Eastern Alps followed the late Early to early Late Cretaceous west to NW directed stacking of Austroalpine units [e.g., *Neubauer et al.*, 1999, and references therein]. It was possibly controlled by the collapse of thickened and gravitational unstable continental crust [*Willingshofer et al.*, 1999a, 1999b] or, alternatively, related to back-arc extension driven by variation in subduction mechanics of the Alpine Tethys [*Froitzheim et al.*, 1997].

6.2. Miocene Extensional Exhumation

Our field structural data have demonstrated the existence of a large array of Miocene normal faults, their geometry following partly the elliptical shape of the Medvednica Mountains. The listric geometry of major faults combined with footwall uplift along associated tectonic omissions (Figure 10) and the local cataclastic deformation overprinting the earlier late Cretaceous detachment demonstrates that significant exhumation occurred during the Miocene extension. The age of this extensional exhumation is confirmed by our AFT age of ~17.3 Ma. The amount of Miocene exhumation of the entire Medvednica Mountains must be in the

range of AFT partial annealing temperatures, but no higher than the ZFT closure temperature; otherwise, the ZFT would have been reset during the Miocene. The amount of differential exhumation between the greenschist facies metamorphic core and regions outside by partly reactivating the earlier ductile detachment cannot be derived by our limited thermochronological data, but our structural interpretation suggest a cumulated footwall exhumation in the range of 2 to 4 km (Figure 9a).

The presence of Miocene detachments and associated extensional exhumation was already documented in the neighboring Miocene basins by the low-angle geometry of normal faults observed in seismic sections [*Tomljenović and Csontos*, 2001] (see also Figure 9). The main depocenter of ~3 km Miocene sediments in the Drava Basin [e.g., *Malvić and Velić*, 2011] is in the direct prolongation of the NE sense of shear documented in the Medvednica Mountains. Miocene detachments associated with extensional exhumation of footwalls are commonly observed in the Dinarides near the Pannonian Basin margin or buried beneath the Miocene sediments in the adjacent part of the Pannonian Basin [*Matenco and Radivojević*, 2012; *Stojadinović et al.*, 2013; *Toljić et al.*, 2013; *Ustaszewski et al.*, 2010]. The range of exhumation ages derived by these studies contains the 20–15 Ma age of enhanced footwall exhumation in the Medvednica Mountains. Similar detachments associated locally with the formation of core complexes are observed near the transition between the Eastern Alps and the Pannonian Basin [*Cao et al.*, 2013; *Fodor et al.*, 2008; *Ratschbacher et al.*, 1990; *Tari et al.*, 1992, 1999]. In general, the asymmetry of the extension is well documented at the scale of the entire Pannonian basin by the formation of the detachments at its margin with the Eastern Alps and Dinarides. Their formation is driven by the rollback of slabs during the evolution of Carpathians and possibly also the Dinarides [*Horváth et al.*, 2006; *Matenco and Radivojević*, 2012].

6.3. Inferences for the Evolution of the Europe-Adria Contact in the Dinarides

Among all extensional structures of the Pannonian Basin, the similarity between the structure of Medvednica Mountains of Croatia and the one of Fruška Gora of Serbia [see *Toljić et al.*, 2013] is remarkable. Both are dome-like inselbergs of roughly the same size surrounded by the Miocene sediments of the Pannonian Basin in the vicinity of Dinarides. Both contain cores composed of greenschist facies rocks metamorphosed during the Cretaceous nappe stacking and have suffered large-scale clockwise rotations during Oligocene-Earliest Miocene times. Both have recorded a two-stage exhumation history of first their metamorphic core and subsequently the entire mountain (Late Cretaceous and Early-Middle Miocene in Medvednica, versus latest Eocene-Early Miocene and Middle Miocene in Fruška Gora, see also *Stojadinović et al.* [2013]). The Miocene exhumation in both areas took place in the vicinity of the Sava zone with kinematics that reactivate its inherited ~NE dipping geometry, an observation already suggested by studies elsewhere in the Dinarides near the contact with the Pannonian Basin [*Ustaszewski et al.*, 2010]. Field relations suggest that the main controlling feature of the Miocene extension in the southern part of the Pannonian Basin was the reactivation of the Europe-Adria suture zone along the length of the entire Dinarides-Pannonian Basin transition up to their contact with the Eastern Alps.

The observation of a late Early Cretaceous metamorphic event and a Late Cretaceous stage of extensional exhumation near the Sava suture in the Medvednica Mountains is a paradox with an obvious solution. In a first instance, it appears to suggest that the Sava Ocean was already closed in this segment of the Dinarides, in contrast with previously proposed latest Cretaceous age of collision [*Schmid et al.*, 2008; *Ustaszewski et al.*, 2009]. The late Cretaceous extension of the Medvednica Mountains is in agreement with the ~100–90 Ma event of low-pressure high-temperature regional metamorphism followed by decompressional melting and emplacement of a granitic pluton at ~82 Ma during a period of crustal uplift, which is observed immediately eastward in the Moslavačka Gora Mountains [*Balen and Petrinec*, 2010; *Balen et al.*, 2001; *Starijaš et al.*, 2010]. However, the earlier closure of the Sava Ocean is contradicted by the observation of late Cretaceous intraoceanic magmatism and the inferred latest Cretaceous age of collision more eastward in the region of Kozara Mountains situated in a central position along the northern Dinaridic border [*Ustaszewski et al.*, 2009]. The obvious solution is the correlation of the late Early Cretaceous metamorphism and Late Cretaceous extensional exhumation in the Medvednica Mountains with coeval and similar well-documented kinematics of the Eastern Alps, rather than the Dinarides. These Eastern Alps processes are imprinted onto the presently neighboring NW Dinaridic margin, i.e., driven by the Alpine evolution of European subduction beneath Adria (Figure 11).

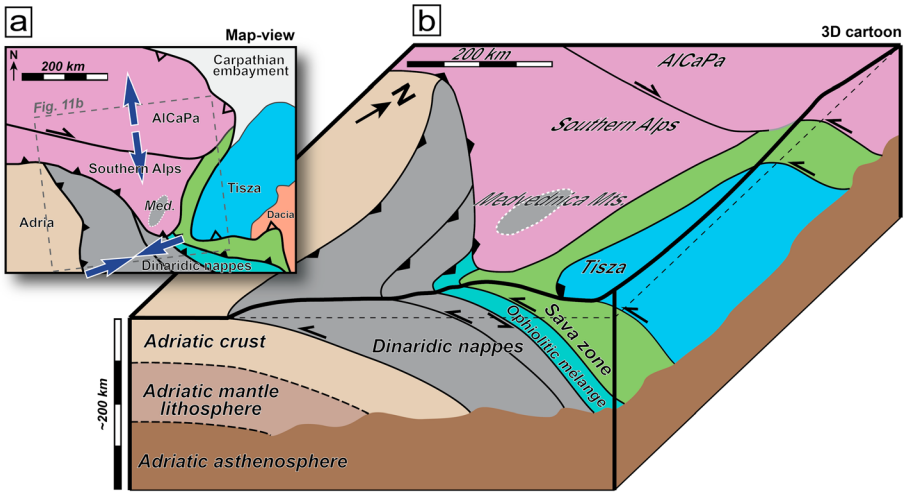

Figure 11. Model for the interaction between the Alps and Dinarides in the larger area of the Medvednica Mountains, for the situation reconstructed at around 20 Ma [modified following an original map reconstruction of *Ustaszewski et al.*, 2008]. (a) Modified map view of the Medvednica Mountains area. Abbreviation: Medvednica Mountains (Med.). (b) Conceptual 3-D cartoon model of the inset as shown in Figure 11a.

6.4. Alps-Dinarides Interference

Our study infers that the interference between the Alpine and Dinaridic tectonic evolutions are larger than previously thought (Figures 1b and 11). In addition to the late Early Cretaceous burial and metamorphism and the Late Cretaceous extension, also the Oligocene-earliest Miocene contraction is likely to be related to Alpine tectonics. Moreover, the allochthonous Žumberak nappe was emplaced with a reconstructed top-south to top-SE kinematics during the Oligocene-earliest Miocene in the SW part of Medvednica Mountains and adjacent parts of the Dinarides across the Miocene Sava basin. This reconstructed kinematics is compatible with the coeval south to SSE-ward retrowedge thrusting that took place in the neighboring Southern Alps starting with Oligocene times [e.g., *Castellarin et al.*, 1992; *Doglioni and Bosellini*, 1987]. Furthermore, the shallow-water Upper Triassic facies of the Žumberak nappe is in contrast with the coeval deep-water facies of all the other Dinaridic internal nappes situated in the vicinity of the Sava zone, east of the Medvednica Mountains. However, a similar nappe contact was inferred in the inselberg situated immediately north of Medvednica, in the Ivanšćica Mountains. Here a late Jurassic-Early Cretaceous Alpine carbonatic platform up to deep-water facies, lacking ophiolites or ophiolitic mélanges, is thrusted over a Triassic-Jurassic shallow- to deep-water facies and an typical internal Dinaridic ophiolitic mélange (Figure 1b) [*Halamić et al.*, 2001]. This nappe contact is likely the same as the Oligocene nappe contact at the base of the Žumberak nappe in the Medvednica Mountains and further SW-ward (Figure 11). This contact has been subsequently affected by the Miocene extension and the Pliocene-Quaternary inversion, causing the earlier Oligocene-earliest Miocene nappe contact to be crosscut and tilted along the Medvednica Mountains extensional dome. This nappe contact is also compatible with a nappe contact observed in western Slovenia, where the Triassic-Cretaceous deep-water facies of the Mid-Slovenian trough of the Tolmin nappe is overthrusted by the Triassic shallow-water facies (including Upper Triassic Dachstein) of the Julian nappe during the Oligocene [e.g., *Celarc et al.*, 2013; *Goričan et al.*, 2012a, 2005, 2012b]. In contrast, the deep-water Tolmin nappe has no record of a possible ophiolitic mélange such as observed in the footwall of the Žumberak nappe (Figure 1). More to the west, the interference between the Eocene Dinaridic top-SW structures and the Alpine top-south thrusting starting with the Oligocene times is a well-known characteristic of the Southern Alps [e.g., *Castellarin and Cantelli*, 2010, and references therein].

Therefore, given all the limitations in structural observations and large-scale correlations, we suggest that the Žumberak nappe of the Medvednica Mountains is a Southern Alps nappe thrusted as a higher unit during Oligocene-earliest Miocene times over the internal Dinarides (Figure 11). In between, it correlates with the upper nappe of the Ivanšćica Mountains and with the Julian nappe, as discussed above. The correlation with the southward retroshearing of the Southern and Julian Alps is in agreement with available quantitative reconstructions that show the position of the Medvednica Mountains was south of the Alps-derived unit (i.e., ALCAPA) at the onset of Miocene extension in the Pannonian Basin [*Ustaszewski et al.*, 2008, Figure 6]. A more

precise correlation with the Southern Alps is still hampered by uncertainties in the paleogeographic position of the Mid-Slovenian trough in the Neotethys Ocean [see *Goričan et al.*, 2012b], the uncertainties in the coeval or postdating large-scale transcurrent to normal faulting offsets of the Periadriatic lineament, and Miocene extension in the regions situated in between Medvednica and the Southern Alps.

6.5. Implications for the Mechanics in Areas of Subduction Polarity Change

Our study infers that areas situated in the zone of interference between two orogens record both their tectonic events, which is a first-order obvious conclusion. In more details, our study shows that the southward to SE-ward thrusting in the eastern part of the Southern Alps during its Oligocene-Early Miocene onset is conditioned by the inherited geometry of the Sava suture zone and the westward prolongation along the Mid-Slovenian trough. This is a rheological weak zone for any deformation postdating its latest Cretaceous-Eocene suturing, as proven by the Sava reactivation along its entire Dinaridic strike by subsequent Miocene detachments. In other words, the existence of a rheological weak zone, such as a sutured subduction zone or a nappe contact, is critical for the localization of orogenic retroshears during their early stages of formation in areas of subduction polarity changes. Such localization is similar with the one observed by far-field strain transmission in rheological weak zones of orogenic forelands, although with an opposite polarity [*Ziegler et al.*, 1995; *Roure*, 2008]. Other examples of contractional polarity changes driven by lateral variations in the rheology or geometry of orogenic systems have been observed and modeled for instance in the Black Sea or the New Guinea-New Britain fore-arc system [*Munteanu et al.*, 2013, 2014]. In all situations, the kinematics of transitional areas is influenced by the geometry of the rheological weak zones and the individual succession of deformation events. It is likely that more examples are to be found worldwide.

7. Conclusions

Our kinematic, depositional, and thermochronological analysis of the Medvednica Mountains has demonstrated two novel stages of extensional exhumation during the Late Cretaceous and Miocene. We have also obtained a number of critical results for the Dinaridic-Alpine junction and for understanding subduction polarity changes in general. In the Medvednica Mountains and neighboring areas, the Late Cretaceous exhumation was accommodated along a large-scale detachment active at ~80 Ma. This detachment largely exhumed the internal core of the mountains that was earlier metamorphosed in greenschist facies during late Early Cretaceous times. As a result of the exhumation, the greenschist facies metamorphic core is brought in direct structural contact with the overlying Paleozoic rocks and their Mesozoic cover. The formation of the detachment was associated with the hanging-wall deposition of Upper Cretaceous sediments, whose gradual transgressive pattern from continental to deep-water facies is almost identical with coeval equivalents found in the Gosau Basins of the Eastern Alps. The Miocene extension has partly reactivated the earlier detachment which resulted in widespread normal faulting and accommodated the second stage of exhumation of the Medvednica Mountains between 20 and 15 Ma. This Miocene extension was characterized by a dominant NE transport direction, which is compatible with similar geometries and transport directions observed elsewhere in the Dinarides and the Alps near their margins with the Pannonian Basin.

Our study shows that the Medvednica Mountains records a tectonic history that combines the typical deformation and associated sedimentation patterns observed in both the Dinarides and the Eastern/Southern Alps. The late Early Cretaceous nappe burial recorded on the Medvednica Mountains is correlated with the deformation that stacked the Austroalpine units of the Eastern Alps. However, it has affected a typical internal Dinaridic sedimentary facies, both being Adria-derived and containing ophiolitic records from the same ocean (i.e., Neotethys). Subsequently, the Late Cretaceous extensional exhumation and associated hanging-wall sedimentation is similar to extensional tectonics and sedimentation observed in the neighboring areas of the Eastern Alps. In contrast, starting with the latest Cretaceous times, the Medvednica Mountains and Eastern Alps were displaced in opposite directions (to the SW and north, respectively) by the different subduction and collision polarities of the Alps and Dinarides. Postdating the Eocene final moment of significant contraction in the Dinarides, the onset of south-vergent Alpine retrowedge thrusting occurred during the Oligocene-Early Miocene and has likely emplaced a Southern Alps nappe as the structural highest unit (i.e., the Žumberak Nappe) in the

Medvednica Mountains and adjacent Dinaridic areas. These deformation stages were subsequently overprinted by the extension, lateral displacements, and inversion driven by the well-known Pannonian back-arc tectonics starting at ~20 Ma. The Miocene extension has affected the Eastern Alps and Dinarides in a similar kinematic way, i.e., by significant footwall exhumation and the formation of core complexes in response to large-scale detachments.

All these findings demonstrate that areas situated near neighboring orogens with different subduction polarities, such as the Medvednica Mountains in between the Alps and the Dinarides, can record a complex and dual tectonic history. The zone of interference is large, not only do structures of the Dinarides extend far into the Southern Alps, but structures of the Eastern and Southern Alps also extend much farther into the Dinarides than previously thought. We suggest that the onset of retrowedge thrusting of the eastern Southern Alps is conditioned by the inherited geometry of the Sava suture zone and the westward prolongation along the Mid-Slovenian trough. In other words, the existence of a rheological weak zone, such as a sutured subduction zone or a nappe contact, is critical for the localization of orogenic retroshears during their early stages of formation in areas of subduction polarity changes.

Acknowledgments
This study is the result of the close collaboration between the Netherlands Research Centre for Integrated Solid Earth Science (ISES) and the Faculty of Mining, Geology and Petroleum of the University of Zagreb (Croatia). Parts of the manuscript are based on the MSc thesis of Anouk Beniest supervised by Inge van Gelder, in particular their common fieldwork and interpretations. Stefan Schmid is gratefully acknowledged for his long-term collaboration and discussions in understanding the structures of the Dinarides and Alps. Dražen Balen is gratefully acknowledged for showing the late Cretaceous magmatic evolution in the Moslavačka Gora Mountains. Lothar Ratschbacher, Gabor Tari, and an anonymous reviewer are gratefully acknowledged for their reviews and suggestions that have significantly improved an earlier manuscript. The data supporting this paper are available by contacting the corresponding author or requesting data from the Utrecht University Tectonics database via uu.teclab@gmail.com.

References

Babić, L., I. Gušić, and J. Zupanic (1976), Paleocene reef-limestone in the region of Banija, Central Croatia, *Geol. Vjesn.*, *29*, 11–47.
Babić, L., A. P. Hochuli, and J. Zupanič (2002), The Jurassic ophiolitic mélange in the NE Dinarides: Dating, internal structure and geotectonic implications, *Eclogae Geolicae Helvetiae*, *95*, 263–275.
Bada, G., F. Horváth, P. Dövényi, P. Szafián, G. Windhoffer, and S. Cloetingh (2007), Present-day stress field and tectonic inversion in the Pannonian basin, *Global Planet. Change*, *58*(1–4), 165–180.
Balen, D., and Z. Petrinec (2010), Complex Cretaceous evolution of the Moslavačka Gora crystalline: Different aspects from various types of "foreign" and "cognate" enclaves inside granites, *Hrvatski geološki kongres Abstracts Book*, *4*, 135–136.
Balen, D., R. Schuster, and V. Garašić (2001), A new contribution to the geochronology of Mt. Moslavačka Gora (Croatia), *PANCARDI 2001: Geodetic and Geophysical Research Institute of the Hungarian Academy of Science*, *2*, 2–3.
Barbarand, J., A. Carter, I. Wood, and T. Hurford (2003), Compositional and structural control of fission-track annealing in apatite, *Chem. Geol.*, *198*(1–2), 107–137.
Basch, O. (1995), Geological map of Medvednica Mt., in *Geološki vodić Medvednice*, edited by K. Šikić, sheet 1, Croatian Geol. Surv. Zagreb, Zagreb.
Belak, M., J. Pamić, T. Kolar-Jurkovšek, Z. Peckay, and D. Karan (1995), Alpinski regional nometamorfni kompleks Medvednice (sjeverozapadna Hrvatska), *Croatian Geol. Surv. Zagreb*, *1. Hrv. geol. kongres*, *Zb. Rad.*, *1*, 67–70.
Bernet, M. (2009), A field-based estimate of the zircon fission-track closure temperature, *Chem. Geol.*, *259*(3–4), 181–189.
Borojević Šostarić, S., F. Neubauer, R. Handler, and L. A. Palinkaš (2012), Tectonothermal history of the basement rocks within the NW Dinarides: New $^{40}Ar/^{39}Ar$ ages and synthesis, *Geol. Carpathica*, *63*(6), 441–452.
Cao, S., F. Neubauer, M. Bernroider, J. Liu, and J. Genser (2013), Structures, microfabrics and textures of the Cordilleran-type Rechnitz metamorphic core complex, Eastern Alps, *Tectonophysics*, *608*, 1201–1225.
Castellarin, A., and L. Cantelli (2010), Geology and evolution of the Northern Adriatic structural triangle between Alps and Apennine, *Rend. Fis. Acc. Lincei*, *21*(1), 3–14.
Castellarin, A., L. Cantelli, A. M. Fesce, J. L. Mercier, V. Picotti, G. A. Pini, G. Prosser, and L. Selli (1992), Alpine compressional tectonics in the Southern Alps. Relationships with the N-Apennines, *Ann. Tect.*, *4*(1), 62–94.
Celarc, B., Š. Goričan, and T. Kolar-Jurkovšek (2013), Middle Triassic carbonate-platform break-up and formation of small-scale half-grabens (Julian and Kamnik-Savinja Alps, Slovenia), *Facies*, *59*, 583–610.
Crnjaković, M. (1980), Sedimentation of transgressive Senonian in Southern Mountain Medvednica, *Geol. Vjesn.*, *32*, 81–95.
Csontos, L., and A. Vörös (2004), Mesozoic plate tectonic reconstruction of the Carpathian region, *Palaeogeogr. Palaeoclimatol. Palaeoecol.*, *210*(1), 1–56.
Dimitrijević, M. D. (1997), *Geology of Yugoslavia*, 2nd ed., 250 pp., Geoinstitute, Belgrade.
Dimitrijevic, M. N., and M. D. Dimitrijevic (1987), *The Turbiditic Basins of Serbia*, 324 pp., Serbian Academy of Sciences and Arts Department of Natural & Mathematical Sciences, Belgrade.
Dodson, M. H. (1973), Closure temperature in cooling geochronological and petrological systems, *Contrib. Mineral. Petrol.*, *40*(3), 259–274.
Doglioni, C., and A. Bosellini (1987), Eoalpine and mesoalpine tectonics in the Southern Alps, *Geol. Rundsch.*, *76*(3), 735–754.
Doglioni, C., P. Harabaglia, S. Merlini, F. Mongelli, A. Peccerillo, and C. Piromallo (1999), Orogens and slabs vs. their direction of subduction, *Earth Sci. Rev.*, *45*(3–4), 167–208.
Ducea, M. N., and J. B. Saleeby (1998), The age and origin of a thick mafic-ultramafic keel from beneath the Sierra Nevada batholith, *Contrib. Mineral. Petrol.*, *133*(1–2), 169–185.
Ducea, M. N., J. Ganguly, E. Rosenberg, P. J. Patchett, W. Cheng, and C. Isachsen (2003), Sm-Nd dating of spatially controlled domains of garnet single crystals: A new method of high temperature thermochronology, *Earth Planet. Sci. Lett.*, *213*, 31–42.
Dunkl, I. (2002), Trackkey: A Windows program for calculation and graphical presentation of fission track data, *Comput. Geosci.*, *28*(1), 3–12.
Đurđanović, Ž. (1973), O paleozoiku i trijasu Medvednice (Zagrebačke gore) i područja Dvora na Uni na temelju konodonta, *Geol. Vjesn.*, *25*, 29–45.
Faccenna, C., C. Piromallo, A. Crespo-Blanc, L. Jolivet, and F. Rosetti (2004), Lateral slab deformation and the origin of the western Mediterranean arcs, *Tectonics*, *23*, TC1012, doi:10.1029/2002TC001488.
Faccenna, C., L. Civetta, M. D'Antonio, F. Funiciello, L. Margheriti, and C. Piromallo (2005), Constraints on mantle circulation around the deforming Calabrian slab, *Geophys. Res. Lett.*, *32*, L06311, doi:10.1029/2004GL021874.
Faccenna, C., T. W. Becker, C. P. Conrad, and L. Husson (2013), Mountain building and mantle dynamics, *Tectonics*, *32*, 1–15, doi:10.1029/2012TC003176.
Filipović, I., D. Jovanović, M. Sudar, P. Pelikán, S. Kovác, G. Less, and K. Hips (2003), Comparison of the Variscan-Early Alpine evolution of the Jadar Block (NW Serbia) and "Bükkium" (NE Hungary) terranes: Some paleogeographic implications, *Slovak Geol. Mag.*, *9*(1), 23–40.

Fodor, L., G. Bada, G. Csillag, E. Horvath, Z. Ruszkiczay-Rudiger, K. Palotas, F. Sikhegyi, G. Timar, and S. Cloetingh (2005), An outline of neotectonic structures and morphotectonics of the western and central Pannonian Basin, *Tectonophysics*, *410*(1–4), 15–41.
Fodor, L., et al. (2008), Miocene emplacement and rapid cooling of the Pohorje pluton at the Alpine-Pannonian-Dinaridic junction, Slovenia, *Swiss J. Geosci.*, *101*(1), 255–271.
Froitzheim, N., P. Conti, and M. van Daalen (1997), Late Cretaceous, synorogenic, low-angle normal faulting along the Schlinig fault (Switzerland, Italy, Austria) and its significance for the tectonics of the Eastern Alps, *Tectonophysics*, *280*(3–4), 267–293.
Fügenschuh, B., N. S. Mancktelow, and D. Seward (2000), The Cretaceous to Neogene cooling and exhumation history of the Oetztal-Stubai basement complex, Eastern Alps: A structural and fission-track study, *Tectonics*, *19*, 905–918, doi:10.1029/2000TC900014.
Galbraith, R. F., and G. M. Laslett (1993), Statistical models for mixed fission track ages, *Nucl. Tracks Radiat. Meas.*, *21*(4), 459–470.
Gleadow, A. J. W. (1981), Fission-track dating methods: What are the real alternatives?, *Nucl. Tracks*, *5*(1–2), 3–14.
Gleadow, A. J. W., and J. F. Lovering (1977), Geometry factor for external detectors in fission track dating, *Nucl. Track Detect.*, *1*(2), 99–106.
Goričan, Š., J. Halamić, T. Grgasović, and T. Kolar-Jurkovšek (2005), Stratigraphic evolution of Triassic arc-backarc system in northwestern Croatia, *Bull. Soc. Geol. Fr.*, *176*(1), 3–22.
Goričan, Š., J. Pavšič, and B. Rožič (2012a), Bajocian to Tithonian age of radiolarian cherts in the Tolmin basin (NW Slovenia), *Bull. Soc. Geol. Fr.*, *183*(4), 369–382.
Goričan, Š., A. Košir, B. Rožič, A. Šmuc, L. Gale, D. Kukoč, B. Celarc, A. E. Črne, T. Kolar-Jurkovšek, and L. Placer (2012b), Mesozoic deep-water basins of the eastern Southern Alps (NW Slovenia), *29th IAS Meeting of Sedimentology*.
Haas, J., and C. Péró (2004), Mesozoic evolution of the Tisza Mega-unit, *Int. J. Earth Sci.*, *93*(2), 297–313.
Haas, J., P. Mioć, J. Pamić, B. Tomljenović, P. Árkai, A. Bérczi-Makk, B. Koroknai, S. Kovács, and E. R. Felgenhauer (2000), Complex structural pattern of the Alpine-Dinaridic-Pannonian triple junction, *Int. J. Earth Sci.*, *89*, 377–389.
Halamić, J., and Š. Goričan (1995), Triassic radiolarites from mountains Kalnik and Medvednica (Northwestern Croatia), *Geol. Croat.*, *48*, 129–146.
Halamić, J., Š. Goričan, D. Slovenec, and T. Kolar-Jurkovsek (1999), Middle Jurassic radiolarite-clastic succession from the Medvednica Mt. (NW Croatia), *Geol. Croat.*, *52*, 29–57.
Halamić, J., V. Marchig, and Š. Goričan (2001), Geochemistry of Triassic Radiolarian cherts in north-western Croatia, *Geol. Carpathica*, *52*, 327–342.
Horváth, F., G. Bada, P. Szafián, G. Tari, A. Ádám, and S. Cloetingh (2006), Formation and deformation of the Pannonian Basin: Constraints from observational data, *Geol. Soc. London Mem.*, *32*(1), 191–206.
Horváth, F., B. Musitz, A. Balazs, A. Vegh, A. Uhrin, A. Nador, B. Koroknai, N. Pap, T. Toth, and G. Worum (2015), Evolution of the Pannonian basin and its geothermal resources, *Geothermics*, *53*, 328–352.
Hurford, A. J., and P. F. Green (1983), Zeta age calibration of fission-track dating, *Chem. Geol.*, *1*(4), 285–317.
Jamičić, D. (2000), Structural deformations in metamorphic rocks of Mt. Medvednica (Croatia), *Nat. Croat.*, *9*(4), 275–296.
Jolivet, L., and C. Faccenna (2000), Mediterranean extension and the Africa-Eurasia collision, *Tectonics*, *19*(6), 1095–1106, doi:10.1029/2000TC900018.
Jolivet, L., V. Famin, C. Mehl, T. Parra, C. Aubourg, R. Hébert, and P. Philippot (2004), Progressive strain localisation, boudinage and extensional metamorphic complexes, the Aegean Sea, *Spec. Pap. Geol. Soc. Am.*, *380*, 185–210.
Judik, K., K. Balogh, D. Tibljaš, and P. Árkai (2006), New age data on the low-temperature regional metamorphism of Mt. Medvednica (Croatia), *Acta Geol. Hung.*, *49*(3), 207–221.
Judik, K., G. Rantitsch, T. M. Rainer, P. Árkai, and B. Tomljenović (2008), Alpine metamorphism of organic matter in metasedimentary rocks from Mt. Medvednica (Croatia), *Swiss J. Geosci.*, *101*(3), 605–616.
Karamata, S. (2006), The geological development of the Balkan Peninsula related to the approach, collision and compression of Gondwanan and Eurasian units, in *Tectonic Development of the Eastern Mediterranean Region*, edited by A. H. F. Robertson and D. Mountrakis, *Geol. Soc. London Spec. Publ.*, 260, 155–178.
Ketcham, R. A. (2005), Forward and Inverse Modeling of Low-Temperature Thermochronometry Data, *Rev. Mineral. Geochem.*, *58*(1), 275–314.
Ketcham, R. A., A. Carter, R. A. Donelick, J. Barbarand, and A. J. Hurford (2007), Improved measurement of fission-track annealing in apatite using *c*-axis projection, *Am. Mineral.*, *92*(5–6), 789–798.
Kilias, A. (2010), *Introduction in Structural Geology (in Greek)*, 2nd revised ed., 440 pp., Olympus, Aristotle Univ. Thessaloniki, Thessaloniki.
Kissling, E., S. M. Schmid, R. Lippitsch, J. Ansorge, and B. Fügenschuh (2006), Lithosphere structure and tectonic evolution of the Alpine arc: New evidence from high-resolution teleseismic tomography, *Geol. Soc. London Mem.*, *32*(1), 129–145.
Krohe, A. (1987), Kinematics of Cretaceous nappe tectonics in the Austroalpine basement of the Koralpe region (eastern Austria), *Tectonophysics*, *136*(3–4), 171–196.
Lister, G. S., and G. A. Davies (1989), The origin of metamorphic core complexes and detachment faults formed during tertiary continental extension in the Northern Colorado River Region, USA, *J. Struct. Geol.*, *11*(1–2), 65–94.
Ludwig, K. R. (2012), Isoplot 3.75: A geochronology toolkit for Microsoft Excel, *Berkeley Geochronology Center*, *Spec. Publ., 5*.
Lugović, B., B. Šegvić, and R. Altherr (2006), Petrology and tectonic significance of greenschists from the Medvednica Mts. (Sava unit, NW Croatia), *Ofioliti*, *31*(1), 39–50.
Luth, S., E. Willingshofer, D. Sokoutis, and S. Cloetingh (2013), Does subduction polarity changes below the Alps? Inferences from analogue modelling, *Tectonophysics*, *582*, 140–161.
Lužar-Oberiter, B., T. Mikes, I. Dunkl, L. Babić, and H. von Eynatten (2012), Provenance of Cretaceous synorogenic sediments from the NW Dinarides (Croatia), *Swiss J. Geosci.*, *105*(3), 377–399.
Magyar, I., D. H. Geary, and P. Muller (1999), Paleogeographic evolution of the Late Miocene Lake Pannon in Central Europe, *Palaeogeogr. Palaeoclimatol. Palaeoecol.*, *147*, 151–167.
Malvić, T., and J. Velić (2011), Neogene tectonics in Croatian part of the Pannonian Basin and reflectance in hydrocarbon accumulations, in *New Frontiers in Tectonic Research—At the Midst of Plate Convergence*, edited by U. Schattner, pp. 215–237, InTech, Rijeka.
Márton, E., D. Pavelić, B. Tomljenović, R. Avanić, J. Pamić, and P. Márton (2002), In the wake of a counterclockwise rotating Adriatic microplate: Neogene paleomagnetic results from northern Croatia, *Int. J. Earth Sci.*, *91*, 514–523.
Matenco, L., and D. Radivojević (2012), On the formation and evolution of the Pannonian Basin: Constraints derived from the structure of the junction area between the Carpathians and Dinarides, *Tectonics*, *31*, TC6007, doi:10.1029/2012TC003206.
Matenco, L., and S. Schmid (1999), Exhumation of the Danubian nappes system (South Carpathians) during the Early Tertiary: Inferences from kinematic and paleostress analysis at the Getic/Danubian nappes contact, *Tectonophysics*, *314*(4), 401–422.
Matenco, L., C. Krézsek, S. Merten, S. Schmid, S. Cloetingh, and P. Andriessen (2010), Characteristics of collisional orogens with low topographic build-up: An example from the Carpathians, *Terra Nova*, *22*(3), 155–165.

Matoš, B., B. Tomljenović, and N. Trenc (2014), Identification of tectonically active areas using DEM: A quantitative morphometric analysis of Mt. Medvednica, NW Croatia, *Geol. Quart.*, *58*(1), 51–70.
Merten, S. (2011), Thermo-tectonic evolution of a convergent orogen with low-topographic build-up: Exhumation and kinematic patterns in the Romanian Carpathians derived from thermochronology, PhD thesis, VU Univ. Amsterdam, 202 pp.
Muller, W. (2003), Strengthening the link between geochronology, textures and petrology, *Earth Planet. Sci. Lett.*, *206*(3–4), 237–251.
Munteanu, I., E. Willingshofer, D. Sokoutis, L. Matenco, C. Dinu, and S. Cloetingh (2013), Transfer of deformation in back-arc basins with a laterally variable rheology: Constraints from analogue modelling of the Balkanides-Western Black Sea inversion, *Tectonophysics*, *602*, 223–236.
Munteanu, I., E. Willingshofer, L. Matenco, D. Sokoutis, and S. Cloetingh (2014), Far-field contractional polarity changes in models and nature, *Earth Planet. Sci. Lett.*, *395*, 101–115.
Neubauer, F., R. D. Dallmeyer, I. Dunkl, and D. Schirnik (1995), Late Cretaceous exhumation of the metamorphic Gleinalm dome, Eastern Alps: Kinematics, cooling history and sedimentary response in a sinistral wrench corridor, *Tectonophysics*, *242*(1–2), 79–98.
Neubauer, F., J. Genser, and R. Handler (1999), The Eastern Alps: Result of a two-stage collision process, *Mitt. Ges. Geol.- Bergbaustud. Oesterr.*, *92*, 117–134.
Ortner, H. (2001), Growing folds and sedimentation of the Gosau Group, Muttekopf, Northern Calcareous Alps, Austria, *Int. J. Earth Sci. (Geol. Rundsch.)*, *90*, 727–739.
Otamendi, J. E., M. N. Ducea, A. M. Tibaldi, G. W. Bergantz, J. D. de la Rosa, and G. I. Vujovich (2009), Generation of tonalitic and dioritic magmas by coupled partial melting of gabbroic and metasedimentary rocks within the deep crust of the Famatinian magmatic arc, Argentina, *J. Petrol.*, *50*(5), 841–873.
Pamić, J. (1984), Triassic magmatism of the Dinarides in Yugoslavia, *Tectonophysics*, *109*(3–4), 273–307.
Pamić, J. (1993), Eoalpine to Neoalpine magmatic and metamorphic processes in the northwestern Vardar Zone, the easternmost Periadriatic Zone and the southwestern Pannonian Basin, *Tectonophysics*, *226*, 503–518.
Pamić, J. (2002), The Sava-Vardar Zone of the Dinarides and Hellenides versus the Vardar Ocean, *Eclogae Geol. Helv.*, *95*(1), 99–113.
Pamić, J., and B. Tomljenović (1998), Basic geologic data from the Croatian part of the Zagorje-Mid Transdanubian zone, *Acta Geol. Hung.*, *41*, 389–400.
Pamić, J., and D. Balen (2001), Tertiary magmatism of the Dinarides and the adjoining South Pannonian Basin: An overview, *Acta Vulcanol.*, *13*(1–2), 9–24.
Pavelić, D. (2001), Tectonostratigraphic model for the North Croatian and North Bosnian sector of the Miocene Pannonian Basin System, *Basin Res.*, *13*, 359–376.
Placer, L. (1999), Contribution to the macrotectonic subdivision of the border region between Southern Alps and External Dinarides, *Geologija*, *41*, 223–255.
Prosser, S. (1993), Rift related depositional system and their seismic expression, in *Tectonics and Seismic Sequence Stratigraphy*, edited by G. D. Williams and A. Dobb, pp. 35–66, Geol. Soc., London.
Ratschbacher, L., J. H. Behrmann, and A. Pahr (1990), Penninic windows at the eastern end of the Alps and their relation to the intra-Carpathian basins, *Tectonophysics*, *172*, 91–105.
Ratschbacher, L., W. Frisch, H. G. Linzer, and O. Merle (1991), Lateral extrusion in the Eastern Alps; Part 2, Structural analysis, *Tectonics*, *10*(2), 257–271, doi:10.1029/90TC02623.
Reiners, P. W., and T. A. Ehlers (2005), *Low-Temperature Thermochronology; Techniques, Interpretations, and Applications*, *Rev. Mineral. Geochem.*, vol. 58, Mineralog. Soc. of Am., Chantilly.
Rögl, F. (1999), Mediterranean and Paratethys. Facts and hypotheses of an Oligocene to Miocene paleogeography, *Geol. Carpathica*, *50*, 339–349.
Roure, F. (2008), Foreland and hinterland basins: What controls their evolution?, *Swiss J. Geosci.*, *101*, 5–29.
Saftić, B., J. Velić, O. Sztanó, G. Juhász, and Ž. Ivković (2003), Tertiary subsurface facies, source rocks and hydrocarbon reservoirs in the SW part of the Pannonian Basin (Northern Croatia and South-Western Hungary), *Geol. Croatica*, *56*, 101–122.
Schefer, S., D. Egli, S. Missoni, D. Bernoulli, H.-J. Gawlick, D. Jovanović, L. Krystyn, R. Lein, S. M. Schmid, and M. Sudar (2011), Triassic sediments in the Internal Dinarides (Kopaonik area, southern Serbia): Stratigraphy, paleogeographic and tectonic significance, *Geol. Carpathica*, *61*(2), 89–109.
Schmid, S. M., and E. Kissling (2000), The arc of the western Alps in the light of geophysical data on deep crustal structure, *Tectonics*, *19*(1), 62–85, doi:10.1029/1999TC900057.
Schmid, S. M., M. S. Boland, and M. S. Paterson (1977), Superplastic flow in fine grained limestone, *Tectonophysics*, *43*, 257–291.
Schmid, S., D. Bernoulli, B. Fügenschuh, L. Matenco, S. Schefer, R. Schuster, M. Tischler, and K. Ustaszewski (2008), The Alpine-Carpathian-Dinaridic orogenic system: Correlation and evolution of tectonic units, *Swiss J. Geosci.*, *101*(1), 139–183.
Šikić, K., O. Basch, and A. Šimunić (1977), *Basic Geological Map of Yugoslavia 1:1000, Sheet Zagreb*, *Croatian Geological Survey Zagreb*, Federal Geol. Inst., Beograd, Belgrade.
Sremac, J., and M. Mihajlović-Pavlović (1983), Graptoliti Medvednice (Zagrebačke gore), *Rad Jugosl. Akad. Znan. Umjet.*, *404*, 65–68.
Starijaš, B., A. Gerdes, D. Balen, D. Tibljaš, and F. Finger (2010), The Moslavačka Gora crystalline massif in Croatia: A Cretaceous heat dome within remnant Ordovician granitoid crust, *Swiss J. Geosci.*, *103*(1), 61–82.
Steininger, F. F., and G. Wessely (1999), From the Tethyan Ocean to the Paratethys Sea: Oligocene to Neogene stratigraphy, paleogeography and paleobiogeography of the circum-Mediterranean region and the Oligocene to Neogene Basin evolution in Austria, *Mitt. Österr. Geol. Ges.*, *92*, 95–116.
Steininger, F. F., C. Muller, and F. Rogl (1988), Correlation of Central Paratethys, Eastern Paratethys, and Mediterranean Neogene stages, in *The Pannonian Basin, a Study in Basin Evolution*, edited by L. H. Royden and F. Horvath, pp. 79–87, AAPG Mem., London.
Stojadinović, U., L. Matenco, P. A. M. Andriessen, M. Toljić, and J. P. T. Foeken (2013), The balance between orogenic building and subsequent extension during the Tertiary evolution of the NE Dinarides: Constraints from low-temperature thermochronology, *Global Planet. Change*, *103*, 19–38.
Tari, G., F. Horvath, and J. Rumpler (1992), Styles of extension in the Pannonian Basin, *Tectonophysics*, *208*(1–3), 203–219.
Tari, G., P. Dövényi, I. Dunkl, F. Horváth, L. Lenkey, M. Stefanescu, P. Szafián, and T. Tóth (1999), Lithospheric structure of the Pannonian basin derived from seismic, gravity and geothermal data, in *The Mediterranean Basins: Tertiary Extension Within the Alpine Orogen*, edited by B. Durand et al., *Geol. Soc., London Spec. Publ.*, *156*, 215–250.
Tari, V. (2002), Evolution of the northern and western Dinarides: A tectonostratigraphic approach, in *Neotectonics and Surface Processes: The Pannonian Basin and Alpine/Carpathian System*, edited by G. Bertotti and S. Cloetingh, pp. 105–120, EGU Stephan Mueller Spec. Publ. Ser., Vienna.
Tari, V., and J. Pamić (1998), Geodynamic evolution of the northern Dinarides and the southern part of the Pannonian Basin, *Tectonophysics*, *297*(1–4), 269–281.

Tari-Kovačić, V., and E. Mrinjek (1994), The Role of palaeogene clastics in the tectonic interpretation of Northern Dalmatia (Southern Croatia), *Geol. Croatica*, *47*, 127–138.
Toljić, M., L. Matenco, M. N. Ducea, U. Stojadinović, J. Milivojević, and N. Đerić (2013), The evolution of a key segment in the Europe-Adria collision: The Fruška Gora of northern Serbia, *Global Planet. Change*, *103*, 39–62.
Tomljenović, B. (2002), Structural characteristics of Medvednica and Samoborsko Gorje Mts., PhD thesis, Univ. of Zagreb, 208 pp.
Tomljenović, B., and L. Csontos (2001), Neogene-Quaternary structures in the border zone between Alps, Dinarides and Pannonian Basin (Hrvatsko Zagorje and Karlovac Basins, Croatia), *Int. J. Earth Sci.*, *90*(3), 560–578.
Tomljenović, B., L. Csontos, E. Márton, and P. Márton (2008), Tectonic evolution of the northwestern Internal Dinarides as constrained by structures and rotation of Medvednica Mountains, North Croatia, *Geol. Soc. London, Spec. Publ.*, *298*(1), 145–167.
Uhrin, A., I. Magyar, and O. Sztano (2009), Effect of basement deformation on the Pannonian sedimentation of the Zala Basin, SW Hungary, *Földtani Közlöny*, *139*, 273–282.
Ustaszewski, K., S. M. Schmid, B. Fügenschuh, M. Tischler, E. Kissling, and W. Spakman (2008), A map-view restoration of the Alpine-Carpathian-Dinaridic system for the Early Miocene, *Swiss J. Geosci.*, *101*(1), 273–294.
Ustaszewski, K., S. M. Schmid, B. Lugovic, R. Schuster, U. Schaltegger, D. Bernoulli, L. Hottinger, A. Kounov, B. Fügenschuh, and S. Schefer (2009), Late Cretaceous intra-oceanic magmatism in the Internal Dinarides (northern Bosnia and Herzegovina): Implications for the collision of the Adriatic and European plates, *Lithos*, *108*(1–4), 106–125.
Ustaszewski, K., A. Kounov, S. M. Schmid, U. Schaltegger, E. Krenn, W. Frank, and B. Fügenschuh (2010), Evolution of the Adria-Europe plate boundary in the northern Dinarides: From continent-continent collision to back-arc extension, *Tectonics*, *29*, TC6017, doi:10.1029/2010TC002668.
Ustaszewski, K., M. Herak, B. Tomljenović, D. Herak, and S. Matej (2014), Neotectonics of the Dinarides-Pannonian Basin transition and possible earthquake sources in the Banja Luka epicentral area, *J. Geodyn.*, *82*, 52–68.
Vrabec, M., and L. Fodor (2005), Late Cenozoic tectonics of Slovenia: Structural styles at the Northeastern corner of the Adriatic microplate, in *The Adria Microplate: GPS Geodesy, Tectonics and Hazards*, edited by N. Pinter et al., pp. 151–168, Springer, Dordrecht.
Wagreich, M., and K. Decker (2001), Sedimentary tectonics and subsidence modelling of the type Upper Cretaceous Gosau basin (Northern Calcareous Alps, Austria), *Int. J. Earth Sci.*, *90*, 714–726.
Wagreich, M., and P. Faupl (1994), Palaeogeography and geodynamic evolution of the Gosau Group of the Northern Calcareous Alps (Late Cretaceous, Eastern Alps, Austria), *Palaeogeogr. Palaeoclimatol. Palaeoecol.*, *110*, 235–254.
Willingshofer, E., F. Neubauer, and S. Cloetingh (1999a), The significance of Gosau-type basins for the late cretaceous tectonic history of the Alpine-Carpathian belt, *Phys. Chem. Earth, Part A*, *24*(8), 687–695.
Willingshofer, E., J. D. van Wees, S. Cloetingh, and F. Neubauer (1999b), Thermomechanical consequences of Cretaceous continent-continent collision in the eastern Alps (Austria)—Insights from two-dimensional modeling, *Tectonics*, *18*(5), 809–826, doi:10.1029/1999TC900017.
Ziegler, P. A., S. Cloetingh, and J. D. van Wees (1995), Dynamics of intra-plate compressional deformation: The Alpine foreland and other examples, *Tectonophysics*, *252*, 7–22.